nature communications

Article

https://doi.org/10.1038/s41467-025-68257-4

The transcription factor HHEX maintains glucocorticoid levels and protects adrenals from androgen-induced lipid depletion

Received: 17 March 2025

Accepted: 17 December 2025

Published online: 11 January 2026

Check for updates

Typhanie Dumontet[1,2] ✉, Kaitlin J. Basham[2,3], Micah C. Foster[2], Emma Silverman[2], Kyle A. Heard[2], Dominque Johnson[2], Chaelin Lee[2], Samuel W. Plaska[4], David T. Breault[5], David Penton[6], Felix Beuschlein[7,8,9], Adina F. Turcu[2], Christopher R. LaPensee[2], Antonio Marcondes Lerario[2] & Gary D. Hammer[2,10,11]

Glucocorticoid-producing cells of the adrenal cortex (*i.e.* zona fasciculata, zF) constitute the critical effectors of the hypothalamic-pituitary-adrenal axis, mediating the mammalian stress response. With glucocorticoids being essential for life, zF dysfunction perturbs multiple organs that participate in optimizing cardiometabolic fitness. The zF forms a dynamic and heterogenous cell population endowed with the capacity to remodel through the engagement of both proliferative and differentiation programs that enable the adrenal to adapt and respond to diverse stressors. However, the mechanisms that sustain such differential responsiveness remain poorly understood. In this study, we resolve the transcriptome of the steroidogenic lineage by scRNA-seq using *Sf1-Cre*^{high}; *Rosa*$^{mT/mG}$ reporter mice. We identify HHEX, a homeodomain protein, as the most enriched transcription factor in glucocorticoid-producing cells. We utilize genetic mouse models to demonstrate that *Hhex* deletion causes glucocorticoid deficiency in male animals. Molecularly, we demonstrate that HHEX is an androgen receptor (AR) target gene, shaping the sexual dimorphism of the adrenal gland by repressing the female transcriptional program at puberty, while also maintaining zF cholesterol ester content by protecting lipid droplets from androgen-induced-lipophagy. Moreover, our study reveals that, in both sexes, HHEX is crucial for maintaining the identity of the innermost adrenocortical cell subpopulation. Specifically, loss of HHEX impairs the expression of *Abcb1b* (P-glycoprotein/MDR1), an efflux pump regulating steroid export and cellular levels of xenobiotics. Together, these data demonstrate that HHEX serves as a multi-functional regulator of post-natal adrenal maturation that is potentiated by androgens.

[1]Training Program in Organogenesis, Center for Cell Plasticity and Organ Design, University of Michigan, Ann Arbor, MI, USA. [2]Department of Internal Medicine, Division of Metabolism, Endocrinology, and Diabetes, University of Michigan, Ann Arbor, MI, USA. [3]Department of Oncological Sciences, Huntsman Cancer Institute, University of Utah, Salt Lake City, UT, USA. [4]Department of Molecular and Integrative Physiology, University of Michigan, Ann Arbor, MI, USA. [5]Division of Endocrinology, Boston Children's Hospital, Boston, MA, USA. [6]Electrophysiology Facility, University of Zurich, Zurich, Switzerland. [7]Department of Endocrinology, Diabetology and Clinical Nutrition, University Hospital of Zurich (USZ) and University of Zurich (UZH), Zurich, Switzerland. [8]Medizinische Klinik und Poliklinik IV, Klinikum der Universität, Ludwig-Maximilians-Universität, Munich, Germany. [9]The LOOP Zurich - Medical Research Center, Zurich, Switzerland. [10]Department of Cell and Molecular Biology, University of Michigan, Ann Arbor, MI, USA. [11]Endocrine Oncology Program, Rogel Cancer Center, University of Michigan, Ann Arbor, MI, USA. ✉e-mail: tdumonte@med.umich.edu

Glucocorticoids (GC) are cholesterol-derived steroid hormones widely known for maintaining glucose homeostasis[1], modulating the immune system[2], and orchestrating the circadian rhythm established by the suprachiasmatic nucleus[3]. Cortisol in humans, and corticosterone in rodents, hold central importance for the body's response to stress by promoting energy mobilization. The precise control of GC production and secretion is vital for restoring homeostasis after stress exposure, primarily through feedback regulation of the hypothalamo-pituitary-adrenal axis (HPA). However, an imbalance in GC production is a characteristic of chronic stress exposure and is associated with adverse outcomes such as depression, cognitive dysfunction[4], susceptibility to infections[5], elevated cardiometabolic morbidity, and increased mortality[6].

Within the adrenal gland, the zona fasciculata (zF) is the major site of GC production. It is characterized by a high content of the steroid precursor, cholesterol, and the expression of *CYP11B1* that encodes the enzyme required for the final step of GC synthesis[7–12]. At the molecular level, the elevation of circulating Adrenocorticotropic Hormone (ACTH) during stress exposure drives adrenal GC production by mobilizing cholesterol stored in lipid droplets in the form of cholesterol esters. The metabolic conversion of free cholesterol moieties into steroid hormones is accomplished by increasing steroidogenic enzyme expression and activity in the mitochondria of zF cells[13,14]. Historically, the zF has been defined as a homogeneous cell population based on the expression of CYP11B1 in all zF cells. However, recent findings have revealed unanticipated heterogeneity within the zF, including differences in proliferative capacities, sex-specific features, and spatial gradients of signaling activity. Refined sequencing techniques have identified discrete populations within the zF, marked by genes such as *Abcb1b*[15], coding a GC exporter, suggesting that GC production and release may be governed by molecularly and functionally specialized cellular subpopulations.

The mechanisms underlying this cellular heterogeneity are intricately linked to signaling gradients, whereby their disruption perturbs steroidogenic cell differentiation and zonal identity resulting in hormonal disorders[16]. Furthermore, pronounced sex differences in mammalian adrenal biology are well documented, mediated in large part by androgen-mediated transcriptional activation of the nuclear androgen receptor (AR). Nevertheless, the molecular programs coordinating sex-dependent and independent zF cellular diversity and their relevance in disease state remains to be deciphered.

Among the potential regulators of adrenal zonation and function, the transcription factor HHEX (Hematopoietically Expressed Homeobox), also known as HEX and Proline-Rich Homeodomain protein, has emerged as a candidate with possible endocrine function. Initially described in the hematopoietic lineage, where it acts as a transcriptional repressor necessary for the maturation and proliferation of definitive hematopoietic progenitors[17–19], HHEX has since been revealed to function as a transcriptional activator in differentiation processes across various organs[20–24], including the pancreas, where it controls the maintenance of somatostatin-secreting delta cell differentiation[25]. Consistent with this role, polymorphisms in the *HHEX* gene have been associated with type 2 diabetes in Genome-Wide Association Studies (GWAS)[26–33]. Meta-analyses have also suggested associations between *HHEX* single-nucleotide polymorphism (SNP, rs2497306) and circulating levels of adrenal-derived dehydroepiandrosterone sulfate (DHEAS)[34,35], suggesting a role for HHEX in adrenal steroidogenesis. Nevertheless, direct functional evidence for HHEX in adrenal cortex biology is lacking.

In this study, we combine single-cell RNA sequencing (scRNA-seq) and in vivo knockout (KO) of candidate genes to uncover factors that orchestrate cellular diversity in the zF and regulate GC production. We demonstrate that HHEX is uniquely expressed in the zF of rodent and human adrenals. Using the mouse as a model organism, we show that loss of HHEX leads to GC deficiency in males. Importantly, in the male adrenal, we find that HHEX protects the inner zF from androgen-induced lipophagy (lipid depletion) at puberty. Molecularly, HHEX exerts both androgen-dependent and independent functions. Using CUT&Tag technology[36], we demonstrate that HHEX is a bona fide AR target gene that shapes the AR-driven sexual dimorphism of the adrenal gland in the zF. Finally, in both male and female mice, HHEX maintains the expression of GC exporter *Abcb1b* in the inner zF at baseline and is necessary for the expansion of the *Abcb1b*-positive cell population during chronic stress.

Results

scRNA-seq reveals heterogeneity within the steroidogenic lineage of the adrenal cortex

To achieve single-cell resolution of the adrenocortical transcriptome, we selectively labeled steroidogenic adrenocortical cells using a transgenic Cre-LoxP approach. We combined *Sf1-Cre*^{high} [37] mice with *Rosa*$^{mT/mG}$ [38] animals to obtain mice expressing fluorescent reporter proteins at the cell membrane (mT/mG) of cells that express or have expressed the transcription factor SF-1 (Steroidogenic Factor 1, also AdBP4, encoded by *NR5A1*) (Fig. 1A). Consistent with previous results using these transgenic mice, only the adrenal cortex was labeled with green fluorescence (mGFP), leaving the capsule and the medulla fluorescent in the red channel (mTomato)[39–41]. We prepared a single-cell suspension from male adrenals by combining mechanical and enzymatic dissociation at low temperatures to preserve the viability of steroidogenic cells and their transcriptional state. Fluorescence-activated cell sorting (FACS) was then used to isolate GFP-positive cells representing the steroidogenic lineage (Fig. 1B). GFP-positive cells include the progenitor populations as well as differentiated cells (zona glomerulosa (zG) and zF cells). Libraries for scRNA-seq were generated using the 10× Genomics platform. Following quality control and filtering out poor-quality cells, a total of 6497 cells from two replicates were retained for subsequent analyses (Supplementary Fig. 1a). A principal component analysis (PCA), considering a gene set of the most variably expressed genes, distinctly separated cells according to their identity. We then annotated 9 clusters according to the expression of known feature genes (Fig. 1C). All cells expressed GFP, demonstrating the successful enrichment of cells belonging to the steroid lineage. As expected, no medulla cells were found in our dataset. Across the dataset, we identified the mineralocorticoid-producing zG based on the expression of *Cyp11b2* (Fig. 1D) and the glucocorticoid-producing zF based on the expression of *Cyp11b1* (Fig. 1E). Among the cells, 35% expressed *Cyp11b2*, 43% expressed *Cyp11b1*, and 13% expressed both. We confirmed the presence of cells co-expressing *Cyp11b2* and *Cyp11b1* transcripts in both sexes by performing RNAscope on serial sections (Fig. 1F and Supplementary Fig. 1b). We identified the proliferative population based on the expression of *mKi67* (Supplementary Fig. 1c) and we found *Shh*-positive cells partially clustering with the zG and the zF cells (Supplementary Fig. 1d). This finding was validated by RNAscope, where we found a portion of *Shh* transcripts in the upper zF cells, specifically in male adrenals (Supplementary Fig. 1e). We confirmed the presence of a recently described unique cell population defined by high expression of *Abcb1b*, *Sbsn*, *Mgst2*, and *Srd5a2* identified by Lopez and colleagues[15], representing 3–5% of the *Cyp11b1*-positive population (Supplementary Fig. 1f). To provide a user-friendly access to this dataset to the scientific community, we used the 10× Genomics' LoupeR package to generate a CLOUPE file that can be easily imported into the 10× Genomics Loupe Browser for data visualization and further exploration (See below "Methods" and "Data availability" sections).

To gain insights into transcripts that underly differences in zonation (zG versus zF) of the cortex and provide a thorough understanding of the zF transcriptome, we analyzed the most enriched genes in zG and zF cell populations (Fig. 1G). Our dataset revealed specific enrichment of previously unrecognized markers in the zG, such as *Ppp2r2b* (a Wnt pathway antagonist), and *Pcdh19* (a proto-

https://doi.org/10.1038/s41467-025-68257-4

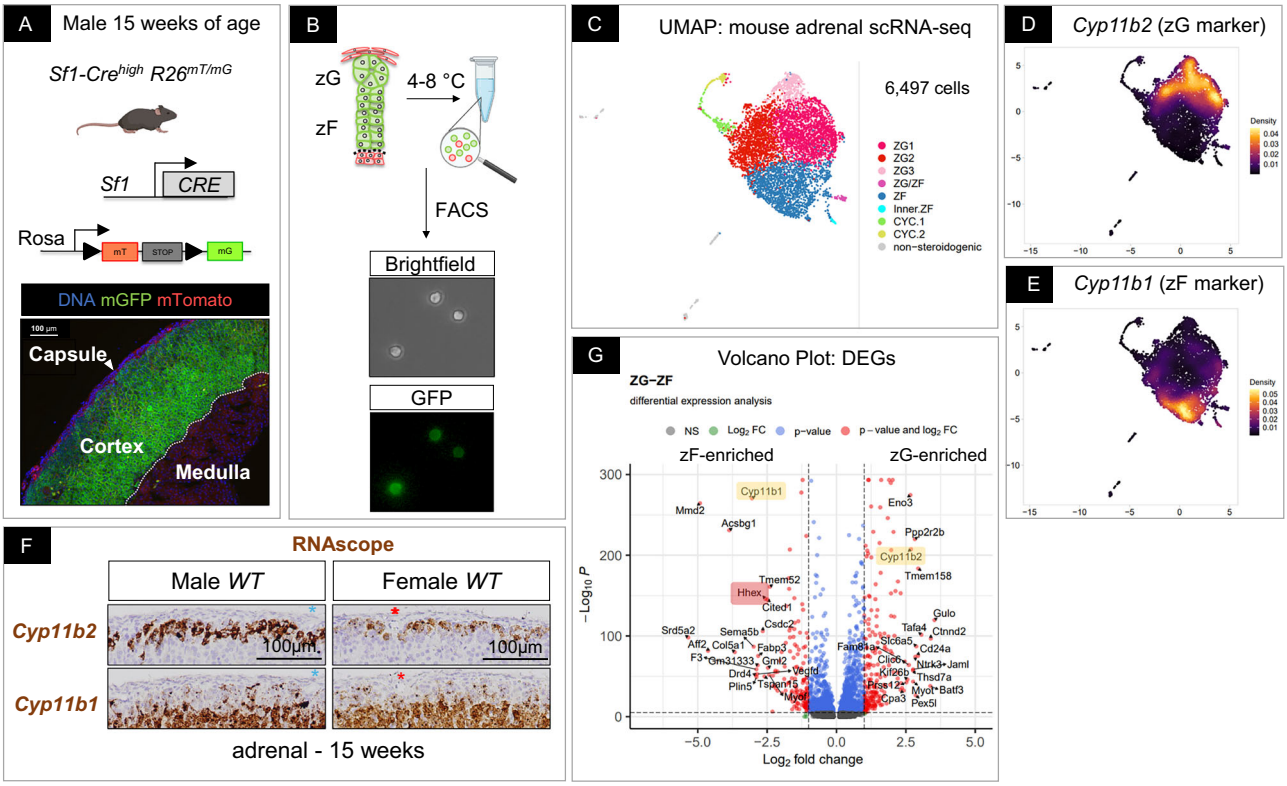

Fig. 1 | scRNA-seq reveals heterogeneity within the steroidogenic lineage of the adrenal cortex. A *Sf1-Cre*^{high} mice were bred with *Rosa*$^{mT/mG}$ mice to label steroidogenic lineage with membrane Green Fluorescent Protein (mG). Non-recombined cells express Tomato (mT). Representative image from a cryosection of an adult male *Sf1-Cre*^{high} *mT/mG* adrenal gland depicting endogenous mGFP (steroidogenic cells) and mTomato fluorescence. Hoechst was used to stain the nuclei. **B** Enzymatic and mechanical single-cell dissociation at low temperature, followed by FACS sorting. The image depicts GFP-positive cells after sorting. **C** UMAP representation of scRNA-seq dataset depicting steroidogenic cell populations in the adult male adrenal ($n = 2$ replicates, 34 adrenals). **D**, **E** Visualization of *Cyp11b2* (**D**) and *Cyp11b1* (**E**) expression in the scRNA-seq dataset. **F** *Cyp11b2* and *Cyp11b1* RNAscope on adrenal serial sections of 15-week-old *WT* male ($n = 5$) and *WT* female ($n = 5$) mice. Nuclei were stained in blue with hematoxylin. Blue and red stars represent capsular arterioles used to image the same area for both transcripts. **G** Volcano Plot representing differentially expressed genes (DEGs) between zG and zF. *p*-values (*p*) were calculated using a non-parametric Wilcoxon rank sum test. *Cyp11b1* and *Cyp11b2* are highlighted in yellow, and *Hhex* is highlighted in red. Created in BioRender. Dumontet, T. (2026) https://BioRender.com/fdp7ezq. FACS Fluorescent-Activated Cell Sorting, GFP Green Fluorescent Protein, UMAP Uniform Manifold Approximation and Projection, NS non-significant, FC Fold change, ZG zona glomerulosa, ZF zona fasciculata, CYC cycling, *WT* Wild Type.

Table 1 | List of zG-enriched transcription factors identified by scRNA-seq

zG-enriched transcription factors			
	avg_log2FC	*p*_val_adj	Main DNA binding domain
Batf3	3.38	1.14E-38	bZIP
Nr4a2	1.96	6.24E-82	Nuclear Receptor
Klf4	1.70	6.17E-26	C2H2 ZF
Jazf1	1.41	6.41E-31	C2H2 ZF
Nr4a1	1.28	2.72E-20	Nuclear Receptor
Klf2	1.24	6.82E-47	C2H2 ZF
Nfatc2	1.12	6.62E-07	Rel
Zfp536	1.17	2.43E-121	C2H2 ZF
Runx1	1.01	3.80E-17	Runt

zG zona glomerulosa, *FC* Fold change, *bZIP* basic Leucine Zipper, *C2H2 ZF* Cys2–His2 zinc finger.

Table 2 | List of zF-enriched transcription factors identified by scRNA-seq

zF-enriched transcription factors			
	avg_log2FC	*p*_val_adj	Main DNA binding domain
Hhex	−2.57	8.67E-147	Homeodomain
Scx	−1.80	1.13E-137	bHLH
Nr1h4	−1.73	7.73E-43	Nuclear Receptor
Epas1	−1.67	7.84E-99	bHLH
Klf15	−1.62	2.07E-30	C2H2 ZF
Dpf3	−1.44	6.44E-14	C2H2 ZF
Fosl2	−1.43	8.28E-88	bZIP
Cebpb	−1.20	3.51E-133	bZIP

zF zona fasciculata, *FC* Fold change, *bHLH* basic helix–loop–helix, *bZIP* basic Leucine Zipper, *C2H2 ZF* Cys2–His2 zinc finger.

cadherin involved in cell-to-cell adhesion) (Supplementary Fig. 1g). Besides the bona fide marker *Cyp11b1*, we found the expression of genes encoding proteins, such as *Mmd2* (a membrane progestin receptor), *Acsbg1* (an acyl-CoA synthetase), and lipid membrane transporters such as *Abca1* (Supplementary Fig. 1h) were enriched in the zF. We then focused our analysis on factors that could directly control gene expression, such as DNA-binding proteins. This analysis identified 9 zG-enriched and 8 zF-enriched transcription factors (Tables 1 and 2). To summarize, our scRNA-seq dataset provides an advanced atlas of the adrenal steroid lineage in the male mouse adrenal, which can be used to identify potential regulators of steroid function.

https://doi.org/10.1038/s41467-025-68257-4

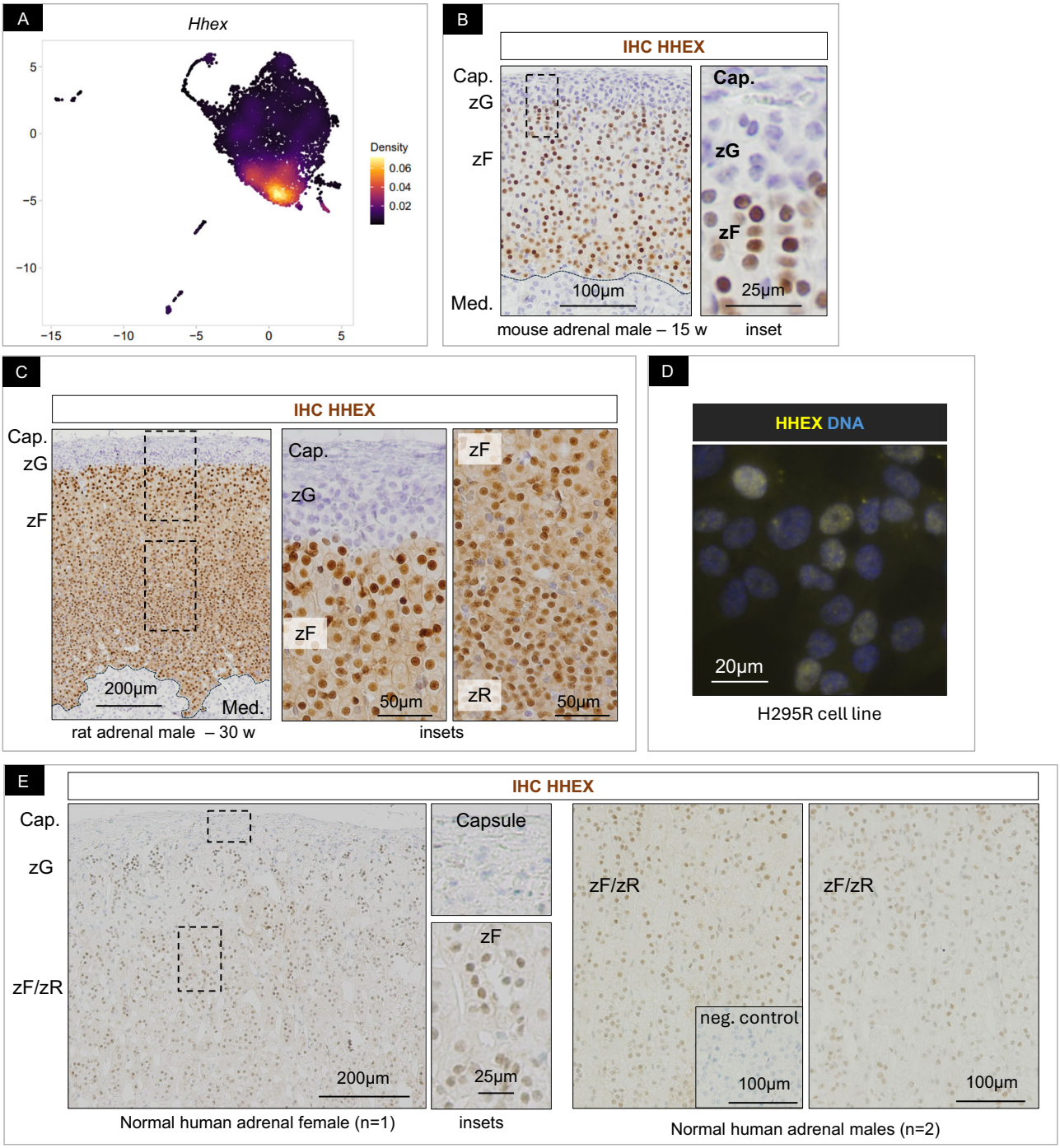

Fig. 2 | scRNAseq identified HHEX as a marker of GCs-producing cells. **A** Visualization of *Hhex* expression in the scRNA-seq dataset. **B**, **C** Expression of HHEX in the male mouse ($n = 5$) (**B**), and male rat ($n = 2$) adrenal glands in brown by immunohistochemistry. Nuclei were stained in blue with hematoxylin. Dotted lines represent the corticomedullary junction. Dotted rectangles depict the insets. **D** Immunofluorescence for HHEX in yellow in the human adrenocortical cell line H295R ($n = 2$). Nuclear counterstain in blue. **E** Expression of HHEX in the human adrenal ($n = 3$). Dotted rectangles depict the insets. IHC immunohistochemistry, Cap. Capsule, zG zona glomerulosa, zF zona fasciculata, zR zona reticularis, Med. medulla, w weeks, neg. negative.

HHEX is a highly conserved marker of glucocorticoid-producing cells

Hhex was identified as the top enriched transcription factor in the zF with an expression pattern mirroring *Cyp11b1* (Fig. 2A). To validate these results, we performed immunohistochemistry and confirmed that HHEX expression was absent from DAB2-positive cells marking the zG (Supplementary Fig. 2a), and was limited to the zF in adult male mouse adrenal (Fig. 2B) and the zF and zR in adult male rat adrenals (Fig. 2C). Using publicly available datasets, we found that human adrenal tissue is among the organs that express the highest levels of *HHEX* (Supplementary Fig. 2b). We also confirmed that HHEX is expressed in the human adrenocortical cell line H295R by immunofluorescence (Fig. 2D) and the zF of the human adrenal cortex (Fig. 2E) by immunohistochemistry. In conclusion, we were able to define HHEX as a marker of the zF that is conserved across species, which supports a potential role in zF function.

https://doi.org/10.1038/s41467-025-68257-4

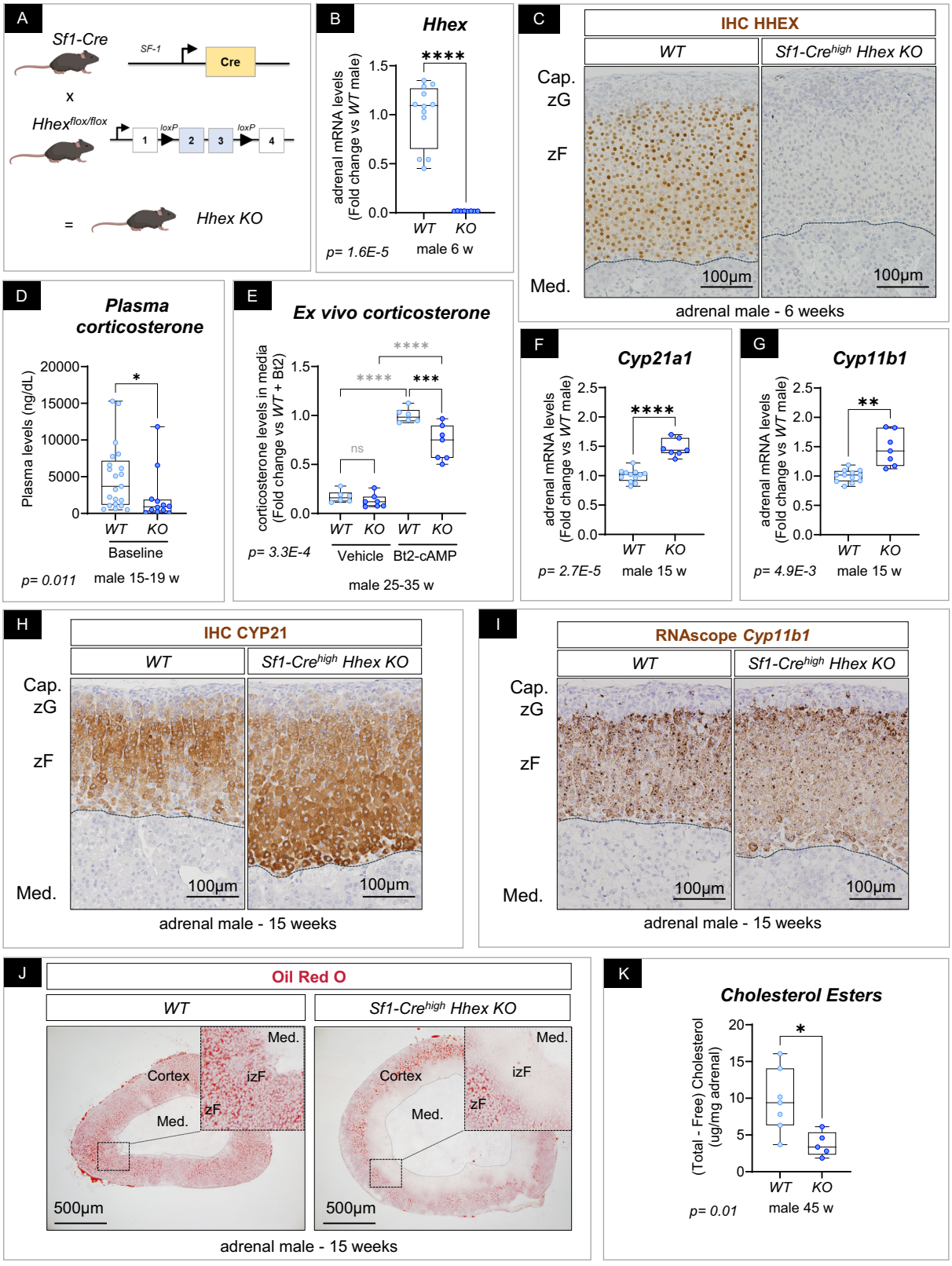

Genetic inactivation of Hhex in the mouse adrenal cortex impairs glucocorticoid levels in males

To gain insights into HHEX function in the adrenal cortex, in vivo, we generated a series of *Hhex KO* models. First, *Hhex*$^{flox/flox}$ mice were crossed with mice expressing *Cre* driven by the *Sf1* promoter[37] to allow for *Hhex* genetic ablation in the entire adrenal cortex from embryonic day E10.5 (*Sf1-Cre*^{high}*; Hhex*$^{flox/flox}$) (Fig. 3A). To analyze the *Sf1-Cre*^{high} *Hhex KO* phenotype, we collected tissue and plasma samples from 6-, 15-, and 50/55-week-old mice for adrenal histology, transcriptomic analysis, and glucocorticoid measurements. Genetic ablation of *Hhex* was validated in 6-week-old mice both by RT-qPCR from mRNAs extracted from whole adrenals and by immunohistochemistry. As

Fig. 3 | *Hhex KO* male mice develop GC deficiency. A Schematic representation of the transgenic mouse models used to inactivate HHEX in adrenocortical cells using *Sf1-Cre*^{high}-mediated recombination of exon 2 and 3 of *Hhex* gene. **B** Quantification of *Hhex* transcripts by RT-qPCR in 6-week-old *WT* (n = 12) and *Sf1-Cre*^{high} *Hhex KO* ($n = 8$) male adrenals. *p*-value (*p*) was calculated using a two-tailed Mann–Whitney test. **C** Expression of HHEX in 6-week-old *WT* ($n = 4$) and *Sf1-Cre*^{high} *Hhex KO* ($n = 4$) male adrenals in brown by immunohistochemistry. Nuclei were stained in blue with hematoxylin. **D** Corticosterone plasma levels of 15–19-week-old *WT* ($n = 21$) and *Sf1-Cre*^{high} *Hhex KO* males ($n = 12$). *p*-value (*p*) was calculated using a two-tailed Mann–Whitney test. (**E**) Ex vivo corticosterone production, released in culture media by adrenal explants after 2.5 h incubation with 2.5 mM of Bt2-cAMP. *WT* ($n = 6$) and *Sf1-Cre*^{high} *Hhex KO* males ($n = 7$). *p*-values (*p*) were calculated using a 2-way ANOVA followed by a Šídák's multiple comparisons test. **F**, **G** Quantification of *Cyp21a1* (**F**) and *Cyp11b1* (**G**) transcripts by RT-qPCR in 15-week-old *WT* ($n = 12$) and *Sf1-Cre*^{high} *Hhex KO* ($n = 7$) male adrenals. *p*-value (*p*) were calculated using a two-tailed unpaired t-test with Welch's correction. (**H**) CYP21A1 immunohistochemistry in adrenals of 15-week-old *WT* ($n = 6$) and *Sf1-Cre*^{high} *Hhex KO* ($n = 6$) male mice. Nuclei were stained in blue with hematoxylin. **I** *Cyp11b1* RNAscope in adrenals of 15-week-old *WT* ($n = 7$) and *Sf1-Cre*^{high} *Hhex KO* ($n = 6$) male mice. Nuclei were stained in blue with hematoxylin. **J** Oil Red O staining of 15-week-old *WT* ($n = 3$) and *Sf1-Cre*^{high} *Hhex KO* ($n = 3$) male adrenals. Dotted rectangles depict the insets. **K** Cholesterol esters quantification in adrenals of 45-week-old *WT* ($n = 7$) and *Sf1-Cre*^{high} *Hhex KO* ($n = 5$) male mice. *p*-value (*p*) was calculated using a two-tailed unpaired t-test with Welch's correction. **B**, **D**–**G**, **K** Graph represents box plots with individual biological replicates, the range (whiskers) and the median (line) within the upper (75%) and lower (25%) quartiles. Source data and exact *p*-values are provided as a Source data file. **C**, **H**, **I**, **J** Dotted lines represent the corticomedullary junction. Created in BioRender. Dumontet, T. (2026) https://BioRender.com/fdp7ezq. IHC immunohistochemistry, Cap. Capsule, zG zona glomerulosa, zF zona fasciculata, izF inner zF, Med. medulla, w weeks, *WT* Wild Type, *KO* Knockout, Bt2-cAMP dibutyryl cyclic adenosine monophosphate, ns non-significant.

anticipated, we observed a significant decrease in *Hhex* expression by RT-qPCR in 6-week-old males (Fig. 3B), and no HHEX staining was observed in *Sf1-Cre*^{high} *Hhex KO* animals by immunohistochemistry (Fig. 3C). Since SF-1 is also expressed in somatic cells of the gonads[37], we assessed HHEX expression in both testis and ovaries. No staining was discernible (Supplementary Fig. 3a), ruling out a major effect of gonadal *Hhex* deletion on the adrenal. At 6 weeks of age the overall zonation of the adrenal cortex was conserved in *Sf1-Cre*^{high} *Hhex KO*, despite cells of the inner zF appearing eosinophilic as illustrated by hematoxylin and eosin staining (Supplementary Fig. 3b). Some cells also displayed hypertrophy, without changes in the adrenal body weight ratio at this age (Supplementary Fig. 3c). At 15-week-old, the hypertrophy was evident and was confirmed by a 32% and 36% decrease in nuclear density in the zF and inner zF respectively (Supplementary Fig. 3d). At 19-week-old, the adrenal body weight ratio was increased by 32% in *Sf1-Cre*^{high} *Hhex KO* (Supplementary Fig. 3e).

To determine if HHEX contributes to zF function, we measured plasma GC levels by mass spectrometry in *WT* (Wild Type) and *Sf1-Cre*^{high} *Hhex KO* mice. We observed a significant 55% decrease in baseline corticosterone in adult males (Fig. 3D). We then cultivated adrenal explants in the presence of dibutyryl-cAMP (Bt2-cAMP) for 2.5 h to stimulate GC production, and observed a 28% decrease in corticosterone levels in media of *Sf1-Cre*^{high} *Hhex KO* compared to *WT* explants (Fig. 3E). These results show that HHEX is required to maintain normal GC production and/or secretion. Despite the fact that the adrenal gland's main function is to produce steroids, adrenal cells do not store GC. Instead, they rapidly metabolize cholesterol and engage the steroidogenic pathway to produce steroids on demand[42–47]. To further interrogate steroidogenic potential in the *Sf1-Cre*^{high} *Hhex KO* adrenals, we assessed the expression of steroidogenic enzymes such as *Cyp21a1* and *Cyp11b1* by RT-qPCR (Fig. 3F, G and Supplementary Fig. 3f–i), and immunohistochemistry for in situ localization (Fig. 3H, I). Surprisingly, we observed an increase in expression and the entire zF was positive for both enzymes. This result made us consider the possibility that GC deficiency was likely a consequence of an upstream defect leading to compensatory upregulation of steroidogenic enzyme gene expression. In support of this hypothesis, corticosteroid precursors such as Progesterone and 11-Deoxycorticosterone plasma levels were indeed significantly decreased (63% and 82% respectively) at baseline in adult males (Supplementary Fig. 3j, k).

To produce steroid hormones on demand, adrenocortical cells metabolize cholesterol (the precursor to all steroids[48,49]). Storage of cholesterol, in the form of lipid droplets (LD), allows for a reservoir of this precursor to be available when needed. Thus, we evaluated cholesterol content in *Sf1-Cre*^{high} *Hhex KO* by detecting neutral lipids such as cholesteryl esters (CE) and triacylglycerol (TG) stored in lipid droplets using Oil Red O staining. By comparing *WT* and *Sf1-Cre*^{high} *Hhex KO* stained adrenal sections, we observed a striking reduction of neutral lipids stored in LD in the inner part of the cortex in 15-week-old *Sf1-Cre*^{high} *Hhex KO* male mice (Fig. 3J). This observation was confirmed by the quantification of intra-adrenal cholesterol esters by colorimetric assay (Fig. 3K), which demonstrated a 61% decrease of CE in the adrenal of 45-week-old *Sf1-Cre*^{high} *Hhex KO* compared to their littermate *WT* controls. Taken together, these results suggest that HHEX is a critical transcription factor that serves to maintain glucocorticoid levels in vivo in males.

Lipid depletion observed in *Hhex KO* male mice results in part from activation of lipophagy in the inner zF

To better understand the mechanisms by which HHEX protects the sterol content of the zF, we interrogated cholesterol ester uptake, lipid droplet catabolism, and de novo synthesis. In rodents, adrenocortical cells obtain extracellular cholesterol mainly through the import of High Density Lipoprotein particles from the circulation[50]. Analysis by immunohistochemistry demonstrated that the inner cortex of *Sf1-Cre*^{high} *Hhex KO* strongly maintained the expression of SR-B1, the receptor for CE-laden HDL particles (Supplementary Fig. 4a), suggesting cholesterol uptake is not perturbed in the inner zF cells of *Sf1-Cre*^{high} *Hhex KO* adrenals. The expression of *Hmgcr*, the rate-controlling enzyme of the mevalonate pathway was significantly upregulated (Supplementary Fig. 4b), suggesting de novo synthesis was not impaired. Taken together, these results indicated that defects in cholesterol uptake and/or synthesis were unlikely the driving mechanism of lipid depletion in *Sf1-Cre*^{high} *Hhex KO*.

To identify potential alternative mechanisms of lipid depletion, we explored the differentially expressed genes in the bulk RNAseq (see below) from male *Sf1-Cre*^{high} *Hhex KO* versus *WT* adrenals, searching for factors involved in lipid catabolism (Supplementary Data 1). The gene *Lipa* (*p*-value = 2.46E-5, Log FC = 1.56) particularly drew our attention for its involvement in the process of acidic lipolysis. Also called "lipophagy", it is defined as the selective engulfment of lipid droplets by the autophagic machinery (Fig. 4A). In brief, this process has been shown to involve the sequestration of lipid droplets by LC3-II positive membranes, where the macroautophagy cargo receptor p62/SQSTM1 bridges LD with the autophagic membrane, the phagophore[51]. The recruitment of p62/SQSTM1 to the LDs is in part mediated by the perilipin PLIN1, an LD-associated protein[52]. Upon fusion with the lysosomes, where the lysosomal acid lipase (LAL) resides, lipid droplets are degraded and cholesterol content recycled. Of note, it has been suggested that Perilipins and p62/SQSTM1 are co-degraded with lipid droplets in lysosomes, whereby their expression is inversely correlated with autophagic activity[51,53,54]. We therefore evaluated the integrity of lipophagy in *WT* and *Sf1-Cre*^{high} *Hhex KO* adrenals. In *WT* adrenals, PLIN1 (Fig. 4B, left) and p62/SQSTM1 staining (Fig. 4C, left) was robust throughout the cortex, while absent in the capsular cells. In *Sf1-Cre*^{high} *Hhex KO*, both PLIN1 and p62/SQSTM1 were markedly

https://doi.org/10.1038/s41467-025-68257-4

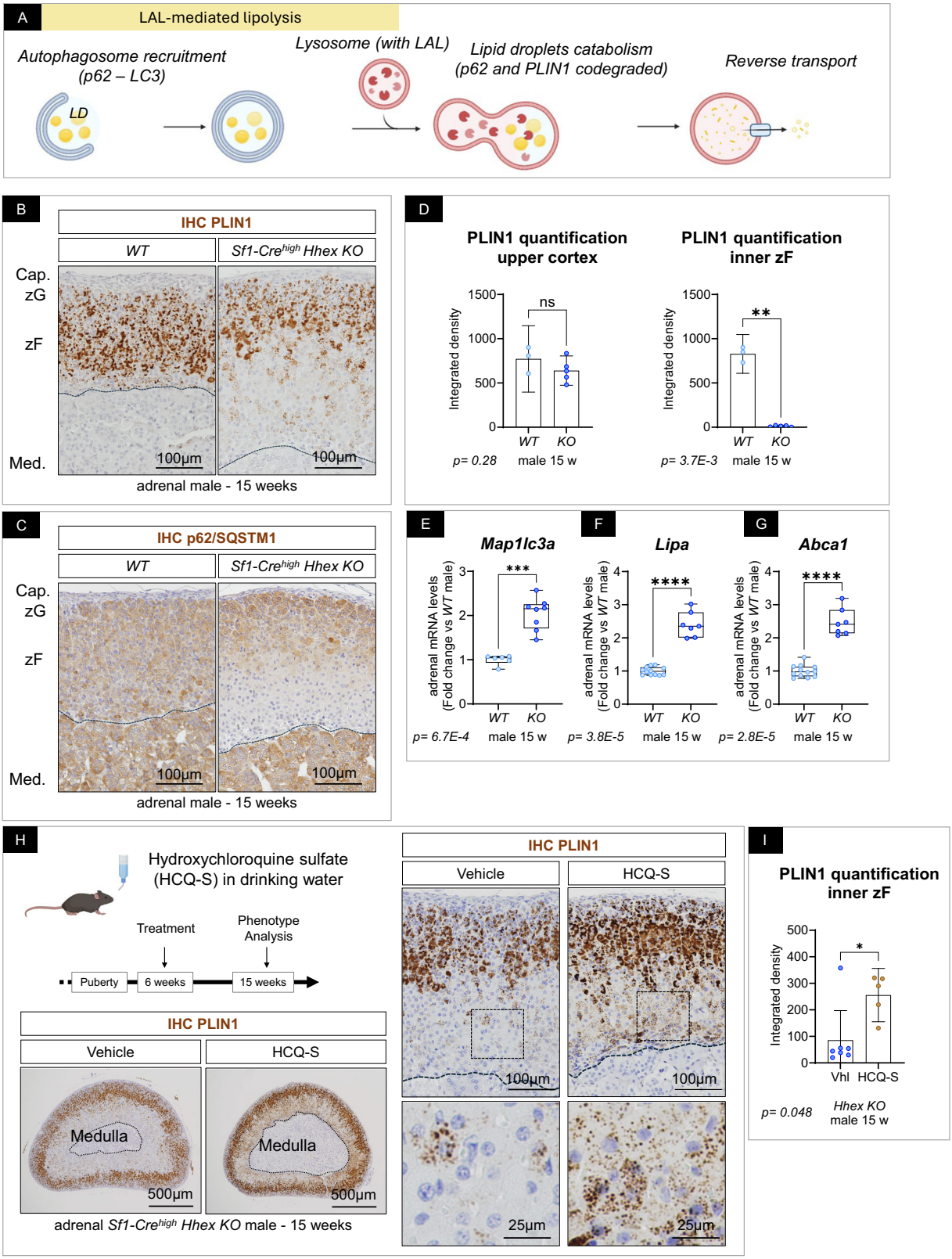

decreased in the inner zone of the cortex (Fig. 4B, C, right), mirroring the lipid-depleted area. Specifically, PLIN1 staining was quantified using image processing analysis (Supplementary Fig. 4c). The inner zF of *Sf1-Cre^{high} Hhex KO* exhibited significantly lower PLIN1 when compared to *WT* adrenals. The upper cortex was not affected in either genotypes (Fig. 4D). Despite the drastic reduction of lipid droplets in the inner zF cells, the mitochondria content was not affected, suggesting that other selective autophagy processes, such as mitophagy, were not activated (Supplementary Fig. 4d). We ruled out the persistence of the X-zone to *Hhex KO* phenotype by deleting *Hhex*, in vivo, using the AS-Cre, which targets the definitive cortex and excludes the X-zone[55]. Similarly to *Sf1-Cre^{high} Hhex KO*, the inner zF of *AS-Cre Hhex KO* was devoid of lipid droplets at 15-week-old (Supplementary Fig. 4e). We also performed RT-PCR for *Pik3c2g*, a robust

Fig. 4 | *Hhex KO* adrenals display signs of activated lipophagy. A Schematic of lipophagy also known as LAL-mediated lipolysis. **B** PLIN1 immunohistochemistry in adrenals of 15-week-old *WT* ($n = 3$) and *Sf1-Cre^{high} Hhex KO* ($n = 5$) male mice. Nuclei were stained in blue with hematoxylin. Dotted lines represent the corticomedullary junction. **C** p62/SQSTM1 immunohistochemistry in adrenals of 15-week-old *WT* ($n = 5$) and *Sf1-Cre^{high} Hhex KO* ($n = 6$) male mice. Nuclei were stained in blue with hematoxylin. Dotted lines represent the corticomedullary junction. **D** Quantification of PLIN1 immunohistochemistry in the upper cortex and inner zF of 15-week-old *WT* ($n = 3$) and *Sf1-Cre^{high} Hhex KO* ($n = 5$) male mice using Fiji. Scatter dot plot represents the mean with 95% confidence interval, and individual biological replicates. *p*-values (*p*) were calculated using a two-tailed unpaired *t*-test with Welch's correction. **E**–**G** Quantification of *Map1lc3a* (**E**) ($n = 6$ *WT* and 8 *Sf1-Cre^{high} Hhex KO*), *Lipa* (**F**) ($n = 12$ *WT* and 7 *Sf1-Cre^{high} Hhex KO*), and *Abca1* (**G**) ($n = 12$ *WT* and 7 *Sf1-Cre^{high} Hhex KO*) transcripts by RT-qPCR in 15-week-old *WT* and *Sf1-Cre^{high} Hhex KO* male adrenals. *p*-values (*p*) were calculated using a two-tailed Mann–Whitney test (*Map1lc3a*) and two-tailed unpaired *t*-tests with Welch's correction (*Lipa* and *Abca1*). **E**–**G** Graph represents box plots with individual biological replicates, the range (whiskers) and the median (line) within the upper (75%) and lower (25%) quartiles. **H** PLIN1 immunohistochemistry in adrenals of *Sf1-Cre^{high} Hhex KO*, vehicle ($n = 7$), and hydroxychloroquine sulfate-treated ($n = 5$) 15-week-old male mice. Nuclei were stained in blue with hematoxylin. Dotted lines represent the corticomedullary junction. Dotted rectangles depict the insets. **I** Quantification of PLIN1 immunohistochemistry in the inner zF using Fiji (Vehicle: $n = 7$, HCQ-S: $n = 5$). Scatter dot plot represents the mean with 95% confidence interval, and individual biological replicates. *p*-value (*p*) was calculated using a two-tailed Mann–Whitney test. Source data and exact *p*-values are provided as a Source data file. Created in BioRender. Dumontet, T. (2026) https://BioRender.com/fdp7ezq. LD lipid droplet, LAL lysosomal acid lipase, IHC immunohistochemistry, Cap. Capsule, zG zona glomerulosa, zF zona fasciculata, Med. medulla, *WT* Wild Type, *KO* Knockout, Vhl vehicle, HCQ-S hydroxychloroquine sulfate, ns non-significant, w weeks.

X-zone marker[56], and could not detect *Pik3c2g* cDNAs in male adrenals from either *WT* and *Sf1-Cre^{high} Hhex KO* genotypes (Supplementary Fig. 4f), indicating that, as expected, the X-zone was absent from both genotypes after puberty.

We confirmed by RT-qPCR the expression of key effectors of lipophagy and observed a significant increase in *Map1lc3a* (encoding the autophagic protein LC3), *Lipa* (encoding the acidic lipase LAL) (Fig. 4E, F) and *Npc2* (encoding a lysosomal protein responsible for cholesterol removal from lysosomes) (Supplementary Fig. 4g) coincident with a marked increase in *Abca1* (encoding a transporter known to limit the intracellular free concentration by promoting cholesterol efflux referred to as reverse cholesterol transport) (Fig. 4G). To test the hypothesis that lipophagy activation contributes to the absence of lipid droplets, we temporally and pharmacologically inhibited autophagy in vivo by treating *WT* and *Sf1-Cre^{high} Hhex KO* mice with hydroxychloroquine sulfate (HCQ-S), which prevents the fusion of the autophagosomes with lysosomes[57]. In *WT*, HCQ-S treatment did not affect the domain of expression of PLIN1 compared to vehicle-treated mice (Supplementary Fig. 4h, i). In contrast, we observed a partial lipid rescue specifically in the inner part of the cortex of *Sf1-Cre^{high} Hhex KO* male mice (Fig. 4H and Supplementary Fig. 4j), which was quantified using image processing analysis (Fig. 4I). However, this partial rescue was not sufficient to restore GC production by adrenal explants, when stimulated with Bt2-cAMP (Supplementary Fig. 4k). Together, these results indicate a crucial role for HHEX in protecting inner zF cells from lipophagy-mediated lipid depletion.

HHEX-dependent lipid depletion and HHEX expression are androgen-mediated

To characterize the temporal dynamic of the LD observed in *Sf1-Cre^{high} Hhex KO* adrenals, we assessed PLIN1 expression by immunohistochemistry at multiple time points (in 2-week-old, 6-week-old, and > 1-year-old mice) (Fig. 5A). The results revealed that the genetic loss of *Hhex* prompted a decrease in lipid droplets in *Sf1-Cre^{high} Hhex KO* male adrenals that became visible at 6 weeks of age. This lipid depletion was noted primarily in the inner zF and expanded over time. With age, the entire zF was substantially lipid-depleted. However, in 2-week-old prepubertal mice, *WT* and *Sf1-Cre^{high} Hhex KO* male adrenals were indiscernible, coincident with intense staining for PLIN1 throughout the cortex in both genotypes. These results indicate that lipid depletion in the *Sf1-Cre^{high} Hhex KO* adrenals begins near puberty and suggests that HHEX is required to actively maintain LD stores from this stage onward. Contrary to what was observed in aged *Sf1-Cre^{high} Hhex KO* male adrenals, we did not observe a drastic LD depletion in females over 1 year of age (Fig. 5A, right). Consistently, when stimulated with Bt2-cAMP, *WT*, and *Sf1-Cre^{high} Hhex KO* female adrenal explants released an equivalent amount of corticosterone into the media (Supplementary Fig. 5a). Of note, we observed that the X-zone was devoid of lipid droplets, which complicated the analysis of the lipid depletion phenotype in females and gonadectomized male mice. To circumvent this issue, we also performed immunohistochemistry for PLIN1 on aged *Sf1-Cre^{high} Hhex KO* females who carried one or more pregnancies resulting in the well-characterized complete regression of the X-zone. We did not observe any loss of lipid droplets in *Sf1-Cre^{high} Hhex KO* primiparous females (Supplementary Fig. 5b).

To explain the decrease of lipid stores observed only in *Sf1-Cre^{high} Hhex KO* males after puberty, we hypothesized an interplay between lipid droplet catabolism and androgen signaling in the adrenal zF. We postulated that the androgenic milieu is the driving force of lipophagy and that HHEX acts as a protective mechanism to maintain LD integrity. To test this hypothesis, we gonadectomized *WT* and *Sf1-Cre^{high} Hhex KO* males at 6 weeks of age, when lipid depletion is first observed, and analyzed the adrenal glands at 15 weeks of age, when LD depletion is observed in the majority of the zF cells in non-gonadectomized *Sf1-Cre^{high} Hhex KO* males. In accordance with our hypothesis, we observed a rescue of lipid droplets in the zF of gonadectomized *Sf1-Cre^{high} Hhex KO*, becoming visually indistinguishable from their gonadectomized *WT* littermates (Fig. 5B). Consistently, p62/SQSTM1 staining was restored in the inner cortex of previously gonadectomized *Sf1-Cre^{high} Hhex KO* (Fig. 5C). Together, these data support the hypothesis that lipid depletion in *Sf1-Cre^{high} Hhex KO* results from an increase in autophagic flux that is specifically the result of androgen-driven lipophagy.

The adrenal glands rely on high cholesterol ester content to support steroidogenesis, which suggests that the catabolic action of the androgens on LD content needs to be tightly controlled. Therefore, we questioned the possible signaling pathways controlling *Hhex* expression. We hypothesized that to protect the LDs at puberty, *Hhex* expression in the male itself might be regulated by androgens. We first looked at the expression of *Hhex* at different time points from birth through aging past 1-year, in both males and females. At the mRNA level, we observed a dramatic increase at puberty, specifically in males (between 3 and 4 weeks of age), resulting in a nine-fold difference between sexes at 6 weeks of age (Fig. 5D). We then proceeded to assess the expression of HHEX in the absence of circulating androgens. We analyzed adrenals from adult gonadectomized male mice and observed a striking decrease in HHEX staining compared to their non-gonadectomized littermates (Fig. 5E). Next, we confirmed the direct contribution of androgens to the upregulation of *Hhex* expression ex vivo while ruling out the participation of gonadotrophins released by the central system. We incubated female adrenal explants with 5a-Androstan-17b-ol-3-one (Dihydrotestosterone, DHT) (an androgen, non-aromatizable into estrogens[58,59]) to activate androgen signaling. Adrenal explants incubated with DHT for 48 h led to a significant 2.2-fold increase in *Hhex* expression compared to the control-treated explants (Supplementary Fig. 5c). This result confirms the direct role of androgens in promoting *Hhex* expression in adrenocortical cells.

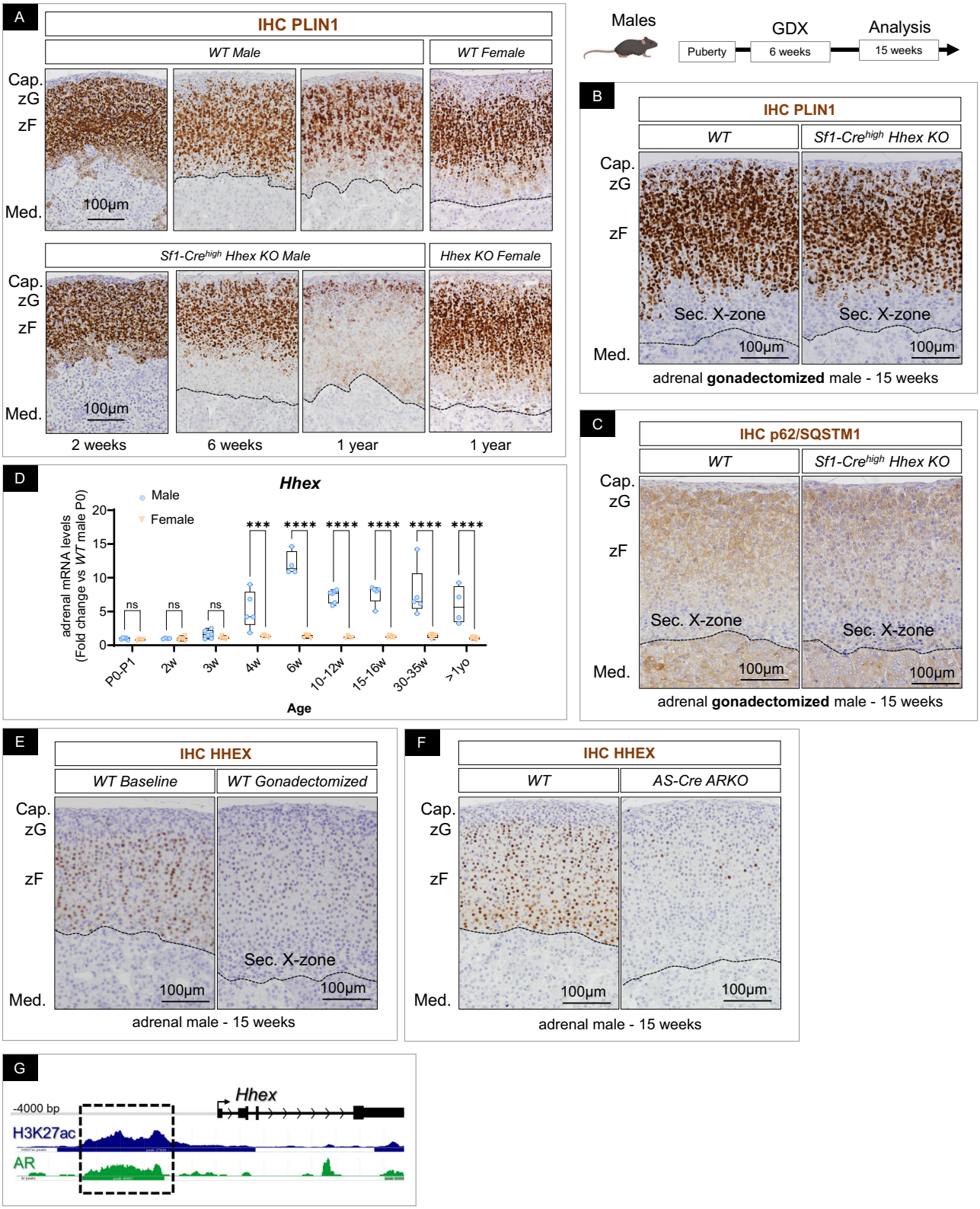

We then tested whether *Hhex* expression is directly regulated through AR signaling, so we proceeded to look at HHEX expression following adrenal-specific AR deletion in the adrenal cortex (*ARKO*) by breeding AR^{flox}/Y[60] mice with *AS-Cre*[55] mice. Similar to our findings upon gonadectomy in *WT* mice, HHEX expression assessed by immunohistochemistry was dramatically reduced in the adrenals of adult adrenal-specific *ARKO* mice (Fig. 5F). Finally, we employed CUT&Tag, a technique based on the same principles as Chromatin Immunoprecipitation (ChIP) that offers the advantage of being more sensitive and requiring less material[36], which makes it suitable to study binding profiles of transcription factors in vivo in the mouse adrenal gland. Using an antibody targeting AR to map genomic AR binding sites in the mouse adrenal, we identified 106726 peaks genome-wide. The distribution profiles showed enrichment of AR binding at transcription start sites (TSS), extending over a 2 kb interval (Supplementary Fig. 5d). At the genome level, AR was mainly distributed in the

Fig. 5 | Lipid depletion in *Hhex KO* male adrenals is androgen-driven. A PLIN1 immunohistochemistry in adrenals of *WT* ($n = 3$) and *Sf1-Cre^{high} Hhex KO* ($n = 3$) adrenals at 2, 6, 15-week-old, and over 1-year-old male and female mice. Nuclei were stained in blue with hematoxylin. Dotted lines represent the corticomedullary junction. **B** PLIN1 immunohistochemistry in adrenals of 15-week-old gonadectomized *WT* ($n = 5$), and *Sf1-Cre^{high} Hhex KO* ($n = 4$) male mice. Nuclei were stained in blue with hematoxylin. Dotted lines represent the corticomedullary junction. **C** p62/SQSTM1 (lipophagy marker) immunohistochemistry in adrenals of 15-week-old gonadectomized *WT* ($n = 5$) and *Sf1-Cre^{high} Hhex KO* ($n = 4$) male mice. Nuclei were stained in blue with hematoxylin. Dotted lines represent the corticomedullary junction. **D** Time course of *Hhex* expression by RT-qPCR in male (circle) and female (triangle) adrenal glands from birth to over 1-year-old. *p*-values (*p*) were calculated using a 2-way ANOVA followed by a Šídák's multiple comparisons test. Graph represents box plots with individual biological replicates, the range (whiskers) and the median (line) within the upper (75%) and lower (25%) quartiles. **E** HHEX expression by immunohistochemistry in the adrenals of 15-week-old *WT* intact ($n = 3$) and gonadectomized ($n = 3$) male adrenals. Nuclei were stained in blue with hematoxylin. Dotted lines represent the corticomedullary junction. **F** HHEX expression by immunohistochemistry in the adrenals of 15-week-old *WT* ($n = 3$) and *AS-Cre ARKO* ($n = 3$) male adrenals. Nuclei were stained in blue with hematoxylin. Dotted lines represent the corticomedullary junction. **G** Histogram depicting the accumulation of androgen receptor (AR) CUT&Tag products obtained from adult male adrenal glands matching the *Hhex* promoter region. H3K27ac is used to identify the open chromatin regions of the genome. Source data and exact *p*-values are provided as a Source data file. Created in BioRender. Dumontet, T. (2026) https://BioRender.com/fdp7ezq. IHC immunohistochemistry, Cap. Capsule, zG zona glomerulosa, zF zona fasciculata, Med. medulla, GDX gonadectomy, Sec. X-zone gonadectomy-induced secondary X-zone, w weeks, yo year-old, P postnatal day, *WT* Wild Type, *KO* Knockout, AS aldosterone synthase, bp base pair, ns non-significant.

intergenic and promoter regions (Supplementary Fig. 5e). This finding underscores the significant role that AR plays in transcriptional regulation in the male mouse adrenal. Next, we conducted motif analysis using HOMER, which showed significant enrichment for Jun-AP1, Fosl2, and Nr5a2 motif (similar to Nr5a1) (Supplementary Data 1). Importantly, AR peaks exhibited significant enrichment for the PGR motif, which carries similarities to steroid receptor binding motifs, including AR. In exploring a possible connection between AR and *Hhex* expression, we identified in *WT* male adrenals an AR peak in the *Hhex* promoter that overlaps with a H3K27ac peak (Fig. 5G). H3K27ac is a histone modification associated with active chromatin, typically found at active enhancers and promoters, indicating potential transcriptional activation. The sexually dimorphic expression of HHEX in the adrenal cortex led us to examine other HHEX-expressing, sexually dimorphic tissues, such as the liver and the pancreas[61,62]. Contrary to the adrenal gland, HHEX was strongly expressed in both male and female hepatocytes (liver), somatostatin-secreting delta cells (pancreas), and hematopoietic cells from the bone marrow, where it was initially identified (Supplementary Fig. 5f). Altogether, these results demonstrate that HHEX is a bona fide AR-target gene in the adrenal zF, which coordinates the precise timing of protecting the integrity of lipid droplets at puberty.

Adrenal sexual dimorphism is partially mediated by HHEX

Recent studies have highlighted the influence of androgens, rather than sex chromosomes, on differentiation, proliferation, and disease development in the adrenal cortex[63–65]. Given the sex differences observed in HHEX expression and the direct transcriptional dependency of HHEX expression on AR, we postulated that HHEX is a mediator of AR actions in the zF, which contributes to sex-biased transcriptional programs in the adrenal cortex. To decipher the transcriptional programs driven by HHEX in the adrenal cortex, we performed bulk RNAseq on adrenals from *WT* and *Sf1-Cre^{high} Hhex KO* mice at 6 weeks of age in both males and females. For a global analysis of gene expression, we performed PCA, a common unsupervised dimensionality-reduction method to visualize and assess the clustering of the data[66]. PCA revealed that over 80% of the variance between the studied mice was explained by the first and second principal components (PCs) that separated individual mice according to sex on the first component (X-axis), and according to genotype on the second component (Y-axis) (Fig. 6A). The clustering suggested that *Hhex* deletion in the steroidogenic lineage drives significant changes at the transcriptome level in the adrenal as soon as 6 weeks of age. To further explore the basis of this change, we examined the differentially expressed genes (DEGs). Using a cut-off of 0.05 for the adjusted *p*-value, the analysis revealed that 3607 genes were differentially expressed between genotypes in males, with only 23 DEGs in females. By analyzing the top DEGs in 6-week-old *Sf1-Cre^{high} Hhex KO* males versus their *WT* littermates (Supplementary Data 1), we observed an enrichment in well-known sexually dimorphic genes[63,67–69], suggesting a feminization of the male transcriptome when *Hhex* is deleted. We confirmed these observations by assessing the expression of "female-biased" *Nr0b1* (known as Dax1) (Fig. 6B), *Frzb* (Fig. 6C), and *Cyp2f2* (Supplementary Fig. 6a, b) in *WT* and *Sf1-Cre^{high} Hhex KO*, male and female, adrenals by RT-qPCR. The sexual dimorphism was completely or at least partially abolished for these three genes in *Sf1-Cre^{high} Hhex KO* male adrenals. In situ, *Nr0b1*-positive cells assessed by RNAscope were observed in the zF of *Sf1-Cre^{high} Hhex KO* male adrenals (similar to *WT* female), while restricted to the zG in *WT* male adrenals, as previously described[69] (Fig. 6D). The expression of *Frzb* was mostly found in cells of the zF in *Sf1-Cre^{high} Hhex KO* (similar to the *WT* female), while absent from the *WT* male zF (Fig. 6E). By quantifying the expression of *Frzb* and *Nr0b1* by RT-qPCR during postnatal life, we observed a striking decrease in males at puberty, which corresponds to the time when *Hhex* expression increases, supporting the role of HHEX in repressing female programs and promoting male programs (Fig. 6F, G). Since testosterone levels (assessed by LC-MSMS) were unchanged in *Sf1-Cre^{high} Hhex KO* compared to *WT* plasma (Supplementary Fig. 6c), we ruled out a contribution of the gonads to the reversal of the sexual dimorphism observed in the adrenal cortex of *Sf1-Cre^{high} Hhex KO* mice. Therefore, we performed immunohistochemistry, and staining revealed high expression of AR in the zF (and to a lesser extent in the zG) (Fig. 6H), which was confirmed by scRNA-seq (Supplementary Fig. 6d). This suggested that the feminization of *Sf1-Cre^{high} Hhex KO* male adrenals could be a result of the loss of androgen signaling directly in the zF. However, *AR* expression assessed by RT-qPCR was not abolished in males *Sf1-Cre^{high} Hhex KO* compared to their littermate controls (Supplementary Fig. 6e), suggesting that HHEX is unlikely upstream of the androgen signaling. To provide a comprehensive analysis, we compared the transcriptome of 6-week-old *Sf1-Cre^{high} Hhex KO* male adrenals and 25-week-old *ARKO* male adrenals and found a significant overlap. Nearly 70% of genes upregulated in *Sf1-Cre^{high} KO* male adrenals belong to the list of upregulated genes in ARKO male adrenals, and 55% belonged to the list of downregulated genes (Fig. 6I and Supplementary Data 1). Taken together, these results suggest that HHEX is a mediator of AR action and that the female transcriptome in the zF is a common program in both sexes before puberty. During the rise of systemic androgen levels concomitant with testis maturation, HHEX expression emerges throughout the zF, which participates to establishing the mature male adrenal transcriptome and consequently institutes an AR:HHEX-dependent sexual dimorphism in the adrenal cortex.

HHEX is crucial for maintaining the identity of the innermost adrenocortical cell subpopulation and promoting *Abcb1b* expression in both sexes

The lower expression of *Hhex* in females compared to males after puberty and the lack of evident LD depletion in female *Sf1-Cre^{high} Hhex*

https://doi.org/10.1038/s41467-025-68257-4

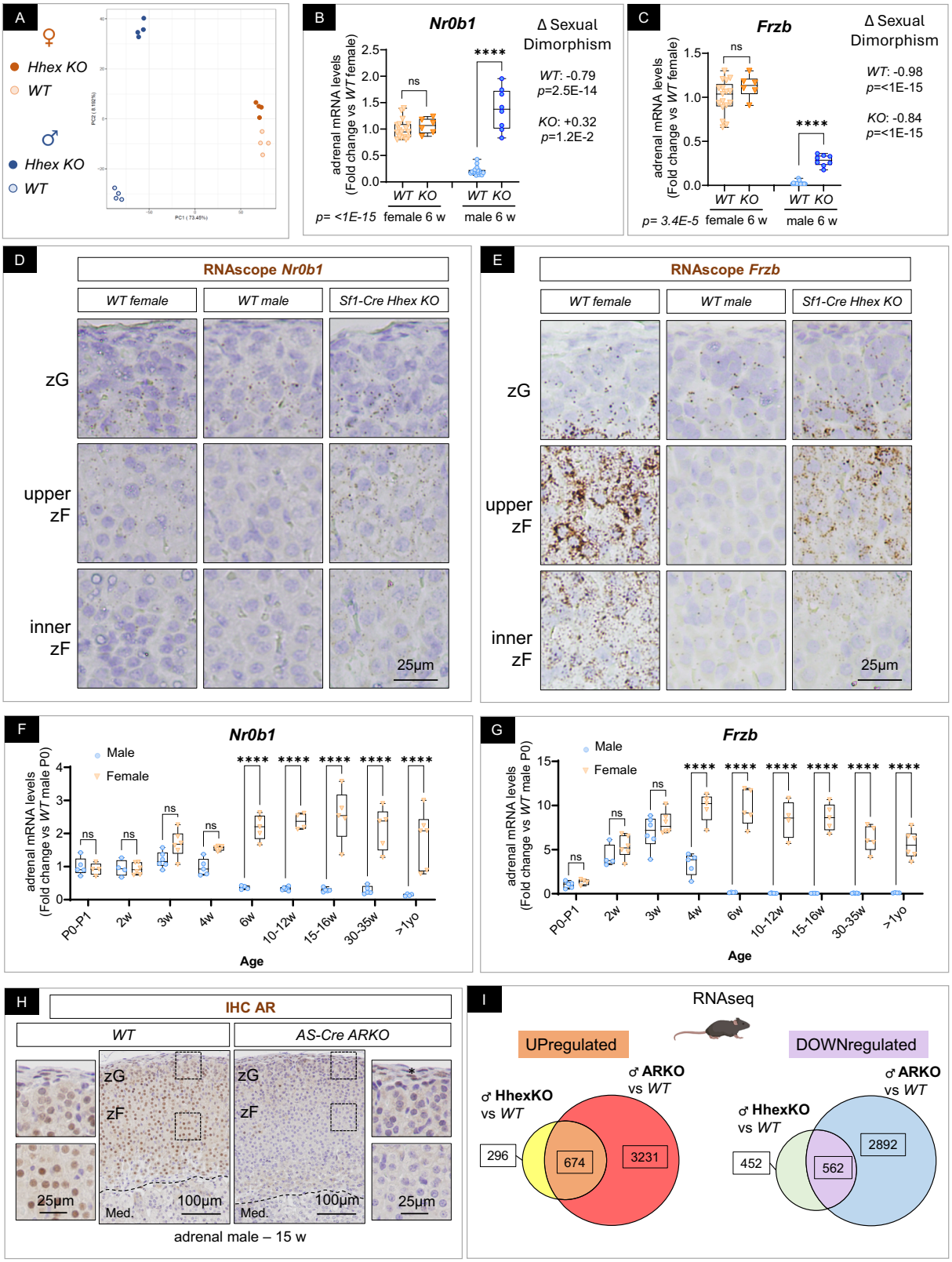

KO mice led us to question whether HHEX contributes to transcriptional programs in the female mouse adrenal cortex. Analysis of HHEX expression by immunohistochemistry in *WT* male and female adrenals revealed a striking lower staining intensity in zF cells of female adrenals (Fig. 7A). Nonetheless, *Hhex* transcript levels were higher in *WT* female adrenals than their *Sf1-Cre*^{high} *Hhex KO* littermates, demonstrating the existence of a baseline expression (albeit lower than male) in female adrenal cells (Fig. 7B). Additionally, bulk RNAseq analysis of 6-week-old female adrenals revealed 23 significant DEGs between *Sf1-Cre*^{high} *Hhex KO* and *WT* mice. Accordingly, the PCA plot demonstrated the separation of female samples based on genotype on the second component of the PCA plot (Fig. 6A), suggesting that HHEX contributes to transcriptional programs in the female adrenal as well. Despite the low number of genes differentially expressed between *WT*

Fig. 6 | HHEX shapes the sexual dimorphism of the transcriptome in the zF. **A** Principal Component Analysis (PCA) plots from bulk RNAseq analysis of 6-week-old *WT* and *Sf1-Cre^{high} Hhex KO* male and female adrenal glands ($n = 4$ for each group). **B**, **C** *Nr0b1* (**B**) and *Frzb* (**C**) expression by RT-qPCR in the adrenal gland of 6-week-old female ($n = 17$ *WT* and 6 *Sf1-Cre^{high} Hhex KO*) and male ($n = 17$ *WT* and 8 *Sf1-Cre^{high} Hhex KO*) mice. *p*-values (*p*) were calculated using a 2-way ANOVA followed by a Šídák's multiple comparisons test. **D**, **E** Expression of *Nr0b1* (**D**) and *Frzb* (**E**) by RNAscope in adrenal glands of 6-week-old *WT* female ($n = 4$) and male ($n = 5$) and *Sf1-Cre^{high} Hhex KO* male ($n = 4$). **F**, **G** Time course of *Nr0b1* (**F**) and *Frzb* (**G**) expression by RT-qPCR in male (circle) and female (triangle) adrenal gland from birth to over 1-year-old. *p*-values (*p*) were calculated using a 2-way ANOVA followed by a Šídák's multiple comparisons test. **B**, **C**, **F**, **G** Graph represents box plots with individual biological replicates, the range (whiskers) and the median (line) within the upper (75%) and lower (25%) quartiles. **H** AR expression by immunohistochemistry in 15-week-old *WT* ($n = 5$) and *ARKO* ($n = 3$) male adrenals. Insets are focusing on capsule/zG cells (top) and zF cells (bottom). Nuclei are counterstained with hematoxylin. Dotted lines represent the corticomedullary junction. Dotted rectangles depict the insets. Asterisk is pointing out AR-positive capsular cells in *ARKO*. **I** Venn diagram of differentially expressed genes in 6-week-old *Sf1-Cre^{high} Hhex KO* and 25-week-old *AS-Cre ARKO* male adrenals compared to their respective *WT*. Source data and exact *p*-values are provided as a Source data file. Created in BioRender. Dumontet, T. (2026) https://BioRender.com/fdp7ezq. PC principal component, *WT* Wild Type, *KO* Knockout, ns non-significant, w weeks, yo year-old, P postnatal day, zG zona glomerulosa, zF zona fasciculata, IHC immunohistochemistry, AS aldosterone synthase, AR androgen receptor.

and *Sf1-Cre^{high} Hhex KO* females, 21 out of 23 were common to DEGs in male *WT* and *Sf1-Cre^{high} Hhex KO*. This included 16 upregulated genes and 5 downregulated genes in *Sf1-Cre^{high} Hhex KO* compared to their respective controls (Fig. 7C). Among them, *Abcb1b* was the most downregulated gene upon *Hhex* deletion, and was further studied based on its established role in sterol flux and stress adaptation in the adrenal cortex[15,70]. Decreased *Abcb1b* expression was further confirmed in larger cohorts, at two time points, in both sexes, using RT-qPCR (35–80% decrease) and RNAscope (Fig. 7D–F). At baseline, we observed that the *Abcb1b* population was localized to the inner zF in *WT* adult mouse adrenals, consistent with previous reports[15]. In females, *Abcb1b* expression was also found in cells of the X-zone (see below). In both sexes, the intensity of the *Abcb1b* staining was visibly reduced in *Sf1-Cre^{high} Hhex KO* adrenals. Based on the decreased expression of *Abcb1b* upon *Hhex* deletion, we thus hypothesized that the expression of other genes uniquely expressed in the inner zF subpopulation might be downregulated with *Hhex* loss. In agreement with this hypothesis, we performed RT-qPCR on *WT* and *Sf1-Cre^{high} Hhex KO* male adrenals and observed a decrease of mRNA levels for other markers of these cells, including *Srd5a2* and *Mgst2* at 6 weeks of age (Supplementary Fig. 7a), suggesting HHEX is required for a unique gene expression profile in this population.

To clarify when HHEX is required for *Abcb1b* expression, we used *Cyp11b1-Cre^{ERT2} Hhex$^{flox/flox}$* and *Cyp11b1-Cre^{ERT2} Hhex$^{wt/wt\ or\ flox/wt}$* (*WT* and *Heterozygotes*) mice fed a tamoxifen chow for 4 weeks after puberty (Supplementary Fig. 7b). This strategy restricted the recombination to the fasciculata lineage upon tamoxifen administration and discriminated defects affecting embryogenesis and/or homeostasis. Similar to the *Sf1-Cre^{high}* model, we observed a significantly decreased expression of *Abcb1b* in the adrenal of *Cyp11b1-Cre^{ERT2} Hhex$^{flox/flox}$* males and females compared to littermate controls (Supplementary Fig. 7c), suggesting that HHEX is necessary for *Abcb1b* expression during homeostasis. This also confirmed that the function of HHEX in promoting *Abcb1b* expression was specific to the adrenal and not to the brain or gonad.

Based on our finding that HHEX promotes *Abcb1b* expression, we hypothesized that the previously described expansion of the *Abcb1b* population in response to chronic stress[15] would be impaired in *Sf1-Cre^{high} Hhex KO* mice. To test this hypothesis, we used long-term ACTH administration as a surrogate for chronic stress exposure[71]. As expected, ACTH induced hyperplasia and hypertrophy in *WT* mice (male and female) and led to significant increases in adrenal body weight ratios in both sexes and both genotypes (Supplementary Fig. 7d, e). Consistent with other in vivo models of chronic stress, we observed by RNAscope a centrifugal expansion of the *Abcb1b* expression domain in the adrenals of both male and female *WT* mice, demonstrating the robustness of this response to HPA axis activation (ACTH response). Under chronic ACTH administration, the *Abcb1b* staining was also visibly reduced in *Sf1-Cre^{high} Hhex KO* compared to *WT* adrenals (Fig. 7F and Supplementary Fig. 7f, right panels). Surprisingly, chronic ACTH administration led to an increased adrenal weight in *Sf1-Cre^{high} Hhex KO* in both sexes despite a failure to increase *Abcb1b* expression, suggesting that expansion of the *Abcb1b* expression domain and zF hyperplasia are two partially uncoupled mechanisms. While the adrenal-specific role of *Abcb1b* is unknown in mice, ABCB1 has been shown to mediate GC release from human adrenal cells[15] and *ABCB1* polymorphism (rs2032582) has been associated with higher cortisol secretion in cortisol-producing adrenal adenomas in humans[72]. Therefore, to assess whether HHEX is contributing to GC release during a chronic stress response, we harvested female *WT* and *Sf1-Cre^{high} Hhex KO* adrenals upon chronic ACTH administration (when *Abcb1b* expression is increased in both sexes). We measured corticosterone released into media by explants and found similar levels between female ACTH-treated *WT* and ACTH-treated *Sf1-Cre^{high} Hhex KO* adrenal explants (Supplementary Fig. 7g). This observation suggests that in females, unlike in males, despite *Hhex* loss and a decrease in *Abcb1b* expression of 46%, residual *Abcb1b* expression may be sufficient to sustain corticosterone release under the conditions tested. Taken together, these results demonstrate that in both sexes, HHEX is required to maintain optimal *Abcb1b* expression in the inner zF, at baseline and upon chronic stress.

Discussion

In the present study, we generated a single-cell RNA seq dataset of the adrenocortical steroidogenic lineage that revealed a marked transcriptome heterogeneity in GC-producing zF cells. We identified the homeobox HHEX as the most enriched transcription factor in the zF and established its role in defining inner zF cell identity. We demonstrated that HHEX is required to protect lipid droplets from androgen-induced lipid depletion and that the loss of HHEX increases lipophagy, leading to decreased steroidogenesis and GC deficiency in vivo in males. We demonstrate that HHEX is a bona fide target gene of the androgen receptor and is highly expressed in the male adrenal, which allows for the repression of female-biased transcriptional programs. Finally, we show that HHEX is required for the expression of the steroid and xenobiotic efflux transporter *Abcb1b* at baseline and in response to chronic stress in both males and females. Therefore, our findings position HHEX as a central integrator of multiple regulatory axes, that synchronizes lipid metabolism, sex hormone signaling, and steroidogenic differentiation.

Our scRNA-seq findings on cells of the steroidogenic lineage are consistent with prior work defining well-known markers of the zG (*Cyp11b2*, *Dab2*, *Lef1*, etc.) and zF (*Cyp11b1*). In our data set, the expression domain of *Shh* included some *Cyp11b2*-positive cells. This is consistent with results obtained using methods with enhanced sensitivity, such as RNAscope[73] and observed in other species[74]. More surprisingly was the existence of *Shh* transcripts in the zF cells, which we confirmed using RNAscope. This apparent discrepancy with earlier reports could be indicative of increased sensitivity of recent methods and reflective of differences in read out used (transcript versus reporter line). Age and sex differences could also contribute to discrepancies found across multiple studies. Indeed, we found that *Shh*

https://doi.org/10.1038/s41467-025-68257-4

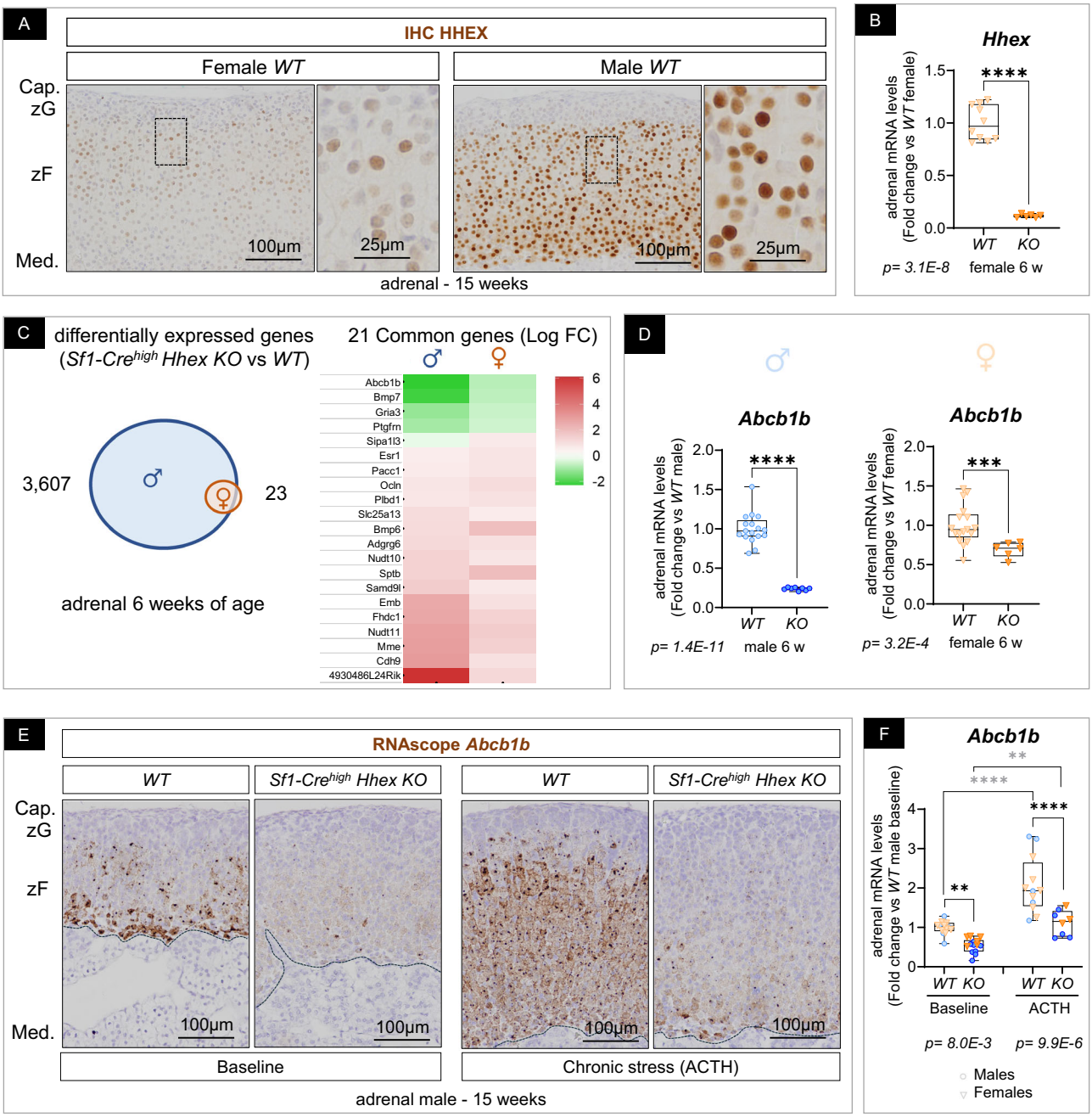

Fig. 7 | HHEX is required for *Abcb1b* expression in the inner zF of both male and female adrenals. A HHEX expression in adult 15-week-old female ($n = 3$) and male ($n = 3$) adrenals by immunohistochemistry. Nuclei are counterstained with hematoxylin. Dotted squares depict the insets. **B** Quantification of *Hhex* transcripts by RT-qPCR in 6-week-old *WT* ($n = 10$) and *Sf1-Cre*^{high} *Hhex KO* ($n = 6$) female adrenals. **C** Venn diagram representing the differentially expressed genes in 6-week-old *Sf1-Cre*^{high} *Hhex KO* adrenals compared to their respective *WT* (males in blue circles and females in orange triangles) and heatmap of commonly differentially expressed genes in males and females *Sf1-Cre*^{high} *Hhex KO*. **D** Quantification of *Abcb1b* transcripts by RT-qPCR in 6-week-old *WT* ($n = 17$ males and 17 females) and *Sf1-Cre*^{high} *Hhex KO* ($n = 8$ males and 6 females) adrenals. *p*-values (*p*) were calculated using a two-tailed unpaired *t*-test with Welch's correction. **E** *Abcb1* expression in 15-week-old *WT* and *Sf1-Cre*^{high} *Hhex KO* male adrenals by RNAscope, at baseline ($n = 4$ *WT* and 4 *Sf1-Cre*^{high} *Hhex KO*) and after chronic stress ($n = 5$ *WT* and 5 *Sf1-Cre*^{high} *Hhex KO*). Nuclei are stained in blue with hematoxylin. Dotted lines represent the corticomedullary junction. **F** Quantification of *Abcb1b* transcripts by RT-qPCR in 15-week-old *WT* and *Sf1-Cre*^{high} *Hhex KO* at baseline ($n = 14$ *WT* and 14 *Sf1-Cre*^{high} *Hhex KO*) and after chronic stress ($n = 12$ *WT* and 8 *Sf1-Cre*^{high} *Hhex KO*) adrenals. *p*-values (*p*) were calculated using a 2-way ANOVA followed by a Šídák's multiple comparisons test. **B**, **D**, **F** Graph represents box plots with individual biological replicates, the range (whiskers) and the median (line) within the upper (75%) and lower (25%) quartiles. Source data and exact *p*-values are provided as a Source data file. IHC immunohistochemistry, Cap. capsule, zG zona glomerulosa, zF zona fasciculata, Med. medulla, *WT* Wild Type, *KO* Knockout, w weeks, FC Fold change, ACTH adrenocorticotropic hormone.

transcripts were easily visualized in the zF cells in male adrenals at 15 weeks of age and were rarely present in the zF of female adrenals. Taken together, these observations represent a potentially important insight into adrenal zonation and plasticity. Further, our results strengthen recent observations that characterized a unique *Abcb1b*$^{+}$/*Sbsn*$^{+}$/*Srd5a2*$^{+}$ population in the inner cortex, and reveal additional zone-specific regulators enriched in the zF (*Mmd2*, *Acsbg1*, and *Abca1*) and zG (*Pp2r2b* and *Pcdh19*). While some prior studies have focused on

adrenal development[75], our study focused on the mouse adult steroidogenic lineage during homeostatic maintenance and identified the zF-specific regulator HHEX. HHEX is a transcription factor that belongs to the family of homeobox proteins that contribute to segmental identity, anterior/posterior patterning of the embryo, mammalian organogenesis, and adult tissue maintenance. Depending on cellular context and cofactor interactions, HHEX functions as a transcriptional repressor or an activator in a tissue-specific manner. In the mouse adrenal, we found that HHEX promotes the expression of *Abcb1b* in the zF but negatively regulates the expression of *Dax1 (Nr0b1)*. *HHEX* SNPs have been repeatedly associated with Type 2 diabetes mellitus. Variants rs1111875 and rs7923837 are associated with impaired insulin secretion and decreased hepatic insulin degradation[76–79]. Other studies revealed a correlation between *HHEX* polymorphisms and metabolic parameters such as triglyceride (rs7923837) and total cholesterol levels (rs2488075 and rs947591)[80]. Relevant to our study, rs2497306 is negatively correlated with levels of DHEAS, a steroid solely produced by the inner human adrenal cortex[34]. While this observation supports our data that HHEX controls steroid output, current mouse models do not permit us to directly assess the role of HHEX in adrenal androgen production (DHEA) because the mouse adrenal cortex does not express cytochrome P450 17α-hydroxylase/17,20 (CYP17) after birth, an enzyme required for androgen synthesis[81]. Importantly, our study lays the groundwork for deciphering the participation of the adrenal gland in the phenotype associated with *HHEX* genetic variants.

In this study, we not only demonstrate that HHEX is required for GC production, we also unmasked the critical role of lipophagy in adrenal lipid droplet catabolism. While the neutral cytoplasmic CE hydrolase HSL, encoded by *Lipe*, has been considered to be the main ester hydrolase in the adrenal[82,83], our findings suggest that conditions exist under which LAL-mediated lipolysis is prevalent. Multiple lines of evidence support that LAL contributes to the regulation of adrenal lipid metabolism. In humans, it has been reported that LAL deficiency accounts for up to 3% of primary pediatric adrenal insufficiency[84,85]. More broadly, LAL mutations are responsible for autosomal recessive cholesteryl ester storage disease (OMIM #27800). The most severe form with complete absence of LAL activity, Wolman disease (OMIM #620151), is usually fatal in the first six months of life. Clinical findings include dyslipidemia, cirrhosis, and calcification of the adrenal[84,86–92], hypothesized to be the accumulation of excess hydrophobic lipids that result in necrosis of adrenal cells and calcification[93]. Our findings that inhibition of lysosomes by HCQ-S partially rescues depletion of lipid droplets in male *Sf1-Cre^{high} Hhex KO* adrenals indicate that macrolipophagy[94], an autophagosome-mediated degradation process, facilitate lipid catabolism in the adrenal cortex. Our results also implicate AR-HHEX signaling in regulating adrenal lipophagy and reveals the sex-specific role of androgen-promoting lipid depletion. Therefore, our mouse model opens an exciting avenue of study focusing on the molecular mechanisms regulating cholesterol metabolism via lipophagy.

In steroidogenic cells, biosynthesis of steroid hormones utilizes cholesterol as a precursor, and in gonads, lipophagy contributes to sex steroid synthesis[95–97]. However, our finding of decreased corticosterone in *Sf1-Cre^{high} Hhex KO* adrenals suggests that lipophagy does not stimulate steroidogenesis. These results implicate lipophagy in the control of hormone synthesis and suggest that activation of lipophagy in the zF could limit adrenal hormone production by restricting cholesterol ester availability for steroidogenesis. Whether excess lipophagy contributes to clinically relevant adrenal insufficiency is unknown. However, cortisol excess is a common feature of adrenocortical carcinoma (ACC), an aggressive form of adrenal cancer, and has been repeatedly associated with poor prognosis among patients[98,99]. Impaired lipophagy and toxic lipid accumulation play a crucial role in the development and progression of multiple diseases, such as atherosclerosis[100–102] and Metabolic Dysfunction-Associated Steatotic Liver Disease[103]. Activation of lipophagy and cholesterol efflux has been proposed as an attractive treatment strategy to prevent cholesterol plaque formation. Lipophagy-inducing compounds have been identified and generated[104] with a number of moieties already clinically approved[105]. Additional studies will be necessary to assess the potential of lipophagy as a promising therapeutic approach to prevent cortisol overproduction in Cushing disease and mild autonomous cortisol secretion, and reduce comorbidities of GC-overproducing adrenal tumors.

We also identified a HHEX-dependent population of inner zF cells in male and female mice that express high levels of *Abcb1b* (also known as MDR1 and P-glycoprotein). Despite the human adrenal gland expressing the highest level of ABCB1, this efflux pump is best known for ensuring blood-brain barrier[70] integrity by preventing the accumulation of toxic levels of xenobiotics and steroids. *Abcb1*-deficient mice exhibit elevated GC in the brain, which is speculated to suppress the HPA axis. Consistent with this notion, *Abcb1*-deficient mice present with lower corticosterone, ACTH, and CRH levels[106]. In humans, polymorphism (rs2032582) in *ABCB1* is associated with decreased HPA axis response (GC levels), and pharmacological inhibition of ABCB1 activity decreases GC release from human adrenocortical cell lines[15] suggesting a role for ABCB1 at the adrenal level in addition to the brain. These findings raise the question as to whether *HHEX* variants account for physiological or subclinical variation in the stress response. However, despite the reduced expression of *Abcb1b* observed in the adrenals of female *Sf1-Cre^{high} Hhex KO*, we found similar corticosterone levels released, which could be indicative of redundant or compensatory mechanisms. Indeed, others ATP transporter, such as ABCC1, have been shown to transport glucocorticoids[70]. It is also possible that ABCB1 protects adrenocortical cells from xenobiotics and drugs. The adrenal cortex expresses many detoxifying enzymes, such as the P450 enzymes, aldo-keto reductases, and glutathione transferases, particularly in the inner cortex. The overlapping expression of ABCB1 suggests multiple mechanisms exist to prevent the accumulation of cytotoxic compounds. In ACC, the lack of efficacy of chemotherapy is thought to be a consequence of increased expression of ABCB1[107]. In vitro ABCB1 inhibition, using Tariquidar or Veparamil, sensitized H295R, a human ACC cell line, to doxorubicin and etoposide[108]. Consequently, modulators of ABCB1 expression, such as HHEX, are promising targets for improving the cytotoxicity of current treatments of ACC and other multidrug-resistant cancer types.

Finally, sex differences are increasingly considered major contributing factors to differences in adrenal disease manifestations, which are more common in females[109]. A more complete understanding of the genetic programs and regulatory factors orchestrating adrenocortical sexual dimorphism will lay the groundwork for future effective sex-specific therapies. The canonical androgenic pathway (via AR/NR3C4) is crucial for the masculinization of zonation and the male-specific transcriptome of the adrenal[63,68,110]. High expression of AR in the zF and weak expression in the zG[69] were confirmed in our study, and sexual dimorphism was partially abolished upon *Hhex* deletion in males, despite sustained *AR* expression and normal levels of circulating androgens. *Sf1-Cre^{high} Hhex KO* and *ARKO* adrenals share many differentially expressed genes, and *Hhex* expression is driven by androgens, indicating that AR engages HHEX to mediate adrenal sexual dimorphism, at least in part by repressing the female transcriptional program. Among the shared differentially expressed genes, *Dax1* is a well-known female-biased gene with high expression in the entire female adrenal cortex and low expression in males (except in the zG)[69]. The *Dax1* expression pattern mirrors the expression of *Hhex* and *Dax1* is repressed at puberty precisely when *Hhex* expression is initiated. Following *Hhex* deletion, *Dax1* expression is increased in the male adrenal to levels comparable to the female adrenal, suggesting that HHEX is a crucial negative regulator of *Dax1* expression. Sex-biased expression of *Dax1* has been shown to be dependent on AR but

independent from its binding to the *Dax1* promoter[69]. Instead, the suppressive action of AR was mainly achieved through SF-1 binding to the *Dax1* promoter. Considering our results, we propose that HHEX is part of this regulatory system, serving as a transcriptional repressor of SF-1-mediated *Dax1* expression in the zF. While the mouse adrenal cortex is recognized as one of the most sexually dimorphic non-reproductive organs, whether and to what extent, this is the case in humans remains unknown. Indeed, contrary to rodents, humans of both sexes produce adrenal androgens, and in pathological conditions such as Congenital Adrenal Hyperplasia and Polycystic Ovary Syndrome, androgens can reach supraphysiological levels. Deciphering the mechanisms by which androgens coordinate sex differences in adrenocortical responsivity/stress adaptation will likely be informative for improved care. Moreover, studies performed in prostate cancer cell lines indicates that *HHEX* locus is also found to be bound by AR and containing androgen response elements[111], raising the possibility that HHEX might mediate the function of other androgen-sensitive cell type. Our study reporting the regulation of the expression of a homeobox protein by androgens in steroidogenic cells of the adrenal gland expands the current knowledge on the regulation of homeobox expression by sex hormones. In conclusion, our work adds to the growing scientific consensus that the adrenal gland is an androgen-sensitive organ and now places HHEX as a major contributor.

To conclude, a better understanding of adrenal cell identity and differentiation is needed for the development of targeted therapy of glucocorticoid-related adrenal disorders. We analyzed cellular diversity in adrenal steroidogenic lineage in mice and identified multiple potential molecular regulators, notably HHEX, which was investigated using conditional KO mice and cutting-edge chromatin accessibility molecular techniques. Our findings reveal that HHEX is crucial for maintaining plasma glucocorticoid levels at baseline in males. We also gleaned additional mechanistic insights into the regulation (by HHEX) of the *Abcb1b*$^{+}$ population, which is crucial for stress adaptation. Overall, our findings add to the existing knowledge involving the function of HHEX in differentiated cells. Its involvement in cholesterol metabolism was completely unknown in the adrenal or any other organs until now. In the adrenal cortex, we demonstrated that HHEX contributes to androgen signaling and participates in the repression of the female transcriptional program in the adrenal. In parallel, its activity protects lipid droplets by preventing androgens from activating lipophagy and triggering lipid depletion in adrenocortical steroidogenic cells. Maintaining cholesterol storage integrity and homeostasis is crucial for adequate steroid release, and our work improves our understanding of the complexity of GC-producing cells. In particular, we lay the groundwork for deciphering the landscape of HHEX functions and provide potential clues to the regulation of lipophagy. Collectively, this information should facilitate cell-targeted therapeutics to treat Cholesteryl ester storage disease (CESD), and other disorders associated with excess lipid storage. GWAS have identified variants of *HHEX* associated with type 2 diabetes, and our work suggests that genetic alterations or variants of expression could be associated with the sensitivity of the adrenal gland to stress response and androgen signaling. Finally, most adrenal diseases do not affect men and women equally. Preclinical biomedical studies have historically focused on male animals, leaving essential questions unanswered. The present study exemplifies how considering sex as a biological variable (SABV) can reveal fundamental molecular mechanisms regulating cellular processes such as lipophagy. We expect the generalization of including SABV when performing experimental studies will improve our understanding of adrenal disease mechanisms.

Limitations of the study

Our research provides a comprehensive single-cell RNAseq dataset of the steroidogenic lineage in the adult male mouse adrenal. However, our downstream functional studies focused solely on HHEX, the identified top transcription factor enriched in the zF. Other proteins and transcription factors enriched in the zG, the zF, and the recently identified *Abcb1b*$^{+}$ cell population remain to be further studied and fully characterized to improve our understanding of the molecular mechanisms modulating steroid production in the adult adrenal cortex. To investigate the role of HHEX in adrenocortical function, we combined genome profiling approaches and transgenic mouse models. Despite a lack of a gain-of-function approach, we generated and phenotyped adrenal-specific *Hhex KO* mouse models of both sexes and at multiple ages. However, *Hhex KO* mice may not inform us of all the possible roles of HHEX in the human adrenal, especially regarding adrenal androgen production. Indeed, functional reticularis cells are absent from rodent species commonly used in a laboratory. Therefore, animal models that better recapitulate human adrenal zonation and steroid production are required for more precise mechanistic and preclinical studies in the future. We also demonstrated that HHEX is expressed in the normal human adrenal of both women and men by immunohistochemistry, but the number of samples was limited and may not allow the accurate assessment of important differences in HHEX expression between sexes, ages, or hormonal status in humans. Finally, our results demonstrate that androgen signaling serves as a potent stimulating signal driving HHEX expression in the adrenal at puberty, but other hormonal factors, such as estrogens, might also influence adrenal functions and were not addressed in the current study.

Methods

Sex as a biological variable

This study examined both male and female mice since sexual dimorphism was observed in the results and therefore studied in the current manuscript.

Mice

Mice were bred in-house and maintained on a C57Bl/6 background at the University of Michigan, USA. They were housed on a 12 h light/12 h dark cycle (lights on at 6 am), at 22.2 °C (72 °F), 35–40% humidity, and fed the commercial rodent chow 5L0D (PicoLab® Laboratory Rodent Diet). Exceptions were made during breeding and before weaning when the Formulab Diet 5008 chow (LabDiet) was used, and during Cre^{ERT2} activation experiments, when mice were placed in a new cage and exclusively fed Teklad Custom TAM diet (400 TC, 2016 - TD.130859, Envigo, expected to provide ~40 mg tamoxifen per kg of body weight per day, assuming 20–25 × *g* body weight and 3–4 × *g* intake). In all experiments (P0 to >1 year old), mice were provided water and food *ad libitum*. At weaning (around 3 weeks of age), mice were separated from parents and kept with same sex littermates at a maximum of five animals per cage. *Hhex*$^{flox/flox}$ mice were purchased at Jackson Laboratory (Stock 025396; B6N.129S1(Cg)-Hhex<tm2Cwb > /J; https://www.jax.org/strain/025396) and initially donated by Dr. Clifford Bogue, M.D., Yale University, USA[112]. They contained loxP sequences flanking exon 2–3 of the *Hhex* mouse gene (ENSMUSG00000024986). *Hhex*$^{flox/flox}$ mice have been previously described and used to successfully delete *Hhex* in the liver[112], pancreas[25,113], osteoclast[114], and myeloid lineage[115]. After cryorecovery, *Hhex*$^{flox/flox}$ mice were crossed with *Sf1-Cre*^{high}*; mT/mG mice*, *AS-Cre; mT/mG*, and *Cyp11b1-Cre*^{ERT2}*; mT/mG* lines. *Sf1-Cre*^{high} mice were provided by the late Dr. Keith Parker, M.D, Ph.D, University of Texas, USA[37]. *Sf1-Cre*^{high} allele harbors five copies of a transgene containing 111 kb of the *Sf1* locus to target Cre expression in various steroidogenic tissues, including the adrenal cortex. This mouse line has been described multiple times to successfully delete various floxed alleles in the adrenal steroidogenic lineage[39–41,64,116–125]. *AS-Cre (Cyp11b2-Cre)* mice were kindly shared by Dr. David Breault, M.D., Ph.D., Harvard, USA[55], and were similarly used to delete various

floxed alleles in the definitive cortex[39,41,63]. *Cyp11b1-Cre*^{ERT2} mice were developed and kindly shared by Dr. Felix Beuschlein, M.D, Zurich, Switzerland. The *Cyp11b1-Cre*^{ERT2} mouse line was generated by PolyGene AG (Rümlang, Switzerland) to establish a Cyp11b1-KO mouse model with a tamoxifen-inducible Cre recombinase (Cre-ERT2) under the gene's control. Exon 2 was selected for inserting the expression cassette, preserving potential regulatory elements in intron 1. To prevent alternative translation initiation, all five ATG start codons in exon 1 were mutated to CTG. The targeting vector included homology arms (4.97 kb and 1.83 kb) generated by PCR from C57Bl/6 N BAC DNA, as well as Cre-ERT2 and β-globin poly(A) sequences assembled via overlap-extension PCR. Additionally, a 1.3 kb fragment containing mutated exon 1, intron 1, and part of exon 2 was synthesized and cloned into the short arm–Cre-ERT2 construct. The final targeting vector, H052.4 TV, incorporated an FRT-flanked neomycin selection cassette and was validated through sequencing. The following primers were used to select positive embryonic stem cell clones H052.17: binds to the elongated short arm of homology 5′-CACGCTGAACTAGCATAGCC-3′ H052.19: binds to the Cre-ERT2 5′-CTACACCAGAGACGGAAATCCATC-3′. *Rosa*$^{mT/mG}$ reporter line[38] has been described multiple times and successfully used to track recombined cells, including steroidogenic cells[39,40,55,63,64,122]. *AR*^{flox} mice[60] were made at the Catholic University of Leuven, Belgium, and kindly shared by Dr. Frank Claessens and Dr. Johan Swinnen.

Rats

Naïve rats were obtained from the animal/rodent redistribution program in place at the University of Michigan and euthanized with CO_2 according to ULAM protocol. Rat adrenals were harvested, fixed, processed, and embedded similarly to the mouse adrenals.

Human adrenal glands

Human adrenal samples were obtained from renal transplantation donors at the University of Michigan. Formalin-fixed paraffin-embedded human adrenal samples without overt pathology based on histologic analysis were used to prepare 5-μm sections that were used for immunohistochemistry. Bulk human tissue gene expression for *HHEX* were obtained from the GTEx portal (GTEx Analysis Release V10 (dbGaP Accession phs000424.v10.p2).

Cells

NCI-H295R cells (ATCC, #CRL-2128, STR profiling) were grown in DMEM/F-12 (GIBCO, #11330032) supplemented with 10% Nu Serum (BD Bioscience, #355100), 1% insulin-transferrin-selenium-ethanolamine (GIBCO, #51500056), and 1% Penicillin-Streptomycin (GIBCO, #15140122).

Genotyping

Mouse tail clips of 2 to 3 mm of length were harvested at weaning, and genomic DNA was extracted using the HotSHOT method[126]. Briefly, tissue was digested in 75 μl of Alkaline Lysis Reagent (25 mM NaOH, 0.2 mM disodium EDTA, pH of 12 without adjusting) for 30 min at 95 °C. Samples were then chilled on ice for 2–3 min, and 75 μl of Neutralization Buffer (40 mM Tris-HCl, pH of 5 without adjusting) were added (Supplementary Data 2). 20 μL PCR reactions were set up in TempAssure 0.2 mL PCR 8 strips color (USA scientific, #1402-4708). For each PCR reaction, 2 μL of genomic DNA were added to a mix comprised of 10 μL of 2× GoTaq® Green Master Mix (Promega, #M7123), combined with 1 μL of each primer (10 μM) and milli Q water for a final volume of 20 μL. Genotyping primer pairs used are listed in Supplementary Data 2. After amplification, PCR products were separated on 2% agarose gels dyed with SYBR Safe (ThermoFischer Scientific, #S33102).

Hormonal manipulation, treatment, and surgery

Chronic ACTH treatment was performed using Synachten 1 mg/mL diluted in PBS 1× (Gibco, #10010023) to 0.25 mg/mL. 13 to 15-week-old male and female mice were injected twice a day intraperitoneally (50 μL) for 10 days. Adrenal enlargement was confirmed at dissection. Testicular gonadectomy was performed using 6-week-old *WT* and *Hhex KO* males. Animals were anesthetized with isoflurane (Fluriso, VetOne) and simultaneously injected with Carprofen (Rimadyl, diluted to 1 mg/mL) at 5 mg/kg for pain relief. Testes were surgically removed, and animals were placed individually in new clean cages after surgery, monitored twice a day for 7–10 days for recovery until suture clips were removed under brief isoflurane anesthesia. At dissection, the regression of seminal vesicles (androgen-sensitive organ) was confirmed, indicating the successful withdrawal of androgen production.

In vivo hydroxychloroquine treatment

Hydroxychloroquine sulfate (HCQ-S, Tokyo Chemical Industry, #H1306) was first resuspended in di-ionized water at a concentration of 6 mg/mL, aliquoted, and stored at −20 °C. HCQ-S was then diluted to a concentration of 0.6 mg/mL with room temperature deionized water (similar to control mice). The solution was administered *ad libitum* in clean water bottles every week. No other liquid source was available during the treatment duration. Based on average water intake, mice were delivered a daily oral dose of 2–4 mg of HCQ-S. Mice were monitored at least weekly.

Tissue harvesting

The day prior to euthanasia, each individual mouse was briefly put on a scale, and the body weight (in grams) was recorded to calculate the adrenal to body weight ratio after euthanasia. At dissection, left adrenal glands were placed in PBS 1× on ice until a precise dissection was performed under a stereo microscope (Nikon, #SMZ800) to remove surrounding fat. Weighing (in milligrams) and imaging (Olympus, #DP21) were quickly recorded to prevent tissue dehydration and lysis. Right adrenals were briefly harvested, dissected from surrounding fat, and immediately snapp frozen in liquid nitrogen for long-term storage at −80 °C.

Mouse adrenal single-cell dissociation and single-cell RNAseq

Adrenal glands were harvested from 15-week-old *Sf1-Cre*^{high}*; Rosa*$^{mT/mG}$ male mice following rapid decapitation to reduce stress-induced transcriptional changes. 14 adrenals (31 mg of tissue) were processed for the first replicate and 20 (49 mg of tissue) for the second. Adrenals were placed immediately into ice-cold 1× Hank's Balanced Salt Solution (HBSS 1×, Thermo Fisher, #14025092) containing calcium and magnesium. 30–50 mg of tissues were then finely chopped in 100–200 μL of HBSS 1× using single-edge razor blades (Persona GEM, #62-0179). From this point, all tips and tubes were precoated with 3% BSA (Roche, #3116956001) in PBS 1× (w/v) to prevent cell loss. Tissue pieces were then transferred to 5 mL tubes (Eppendorf, #0030119487) containing 2 mL of cold HBSS 1× supplemented with 10% Fetal Bovine Serum (Corning, #35-010-CV) and centrifuged for 5 min at 4 °C at 500 × *g* and supernatant was pipetted out and discarded. Single cell suspension was then obtained at low temperature (4 to 10 °C) by combining enzymatic and mechanic dissociation according to the following steps. Mix 1, containing 1900 μL of Buffer X (Mitenyi Biotec, #130-092-628), 50 μL of Papain (Mitenyi Biotec, #130-092-628), and 20 μL of collagenase (Sigma-Aldrich, #C2139) prepared at a concentration of 100 mg/mL in DMEM-12, was added to the tissue preparation and incubated for 15 min at low temperature. Mix 2 (10 μL of enzyme A and 20 μL of Buffer Y, Mitenyi Biotec, #130-092-628) was added to the digestive solution for 1 h from this step. During the dissociation, the cell suspension was gently agitated with mechanical pipetting every

10 min and visually assessed under a microscope for 1 h until the tissue was fully digested. The suspension was then filtered through 70 µm filters (PluriSelect USA, #43-10070-40) to obtain a single cell suspension, and enzymes were neutralized using HBSS 1× containing 10% Fetal Bovine Serum. Red blood cells were removed using Red Blood Cell Lysis buffer (Roche, #11814389001) according to manufacturer guidelines (15 min on orbital shaker in a cold room), and the cells were washed twice in HBSS containing 2% FBS before counting. After final centrifugation, cells were resuspended in 1 mL of HBSS 1×, FBS 2%. Following dissociation, cells were stained with 2 µg/ml DAPI and 5 µM Vybrant DyeCycle Ruby (Invitrogen, #V10309). Ruby-positive, DAPI-negative single cells were sorted based on fluorescent properties using the Thermofisher Bigfoot Cell Sorter at the University of Michigan Flow Cytometry Core. Gating strategy is described in Supplementary Data 1. Cells were collected in BSA-precoated tubes containing HBSS 1× with 2% FBS and kept on ice. Single-cell droplets with a target capture of 10,000 cells were immediately prepared on the 10× Chromium system at the Advanced Genomic Core. Single-cell libraries were prepared using the Chromium Next GEM Single Cell 3′ Gene Expression Library Construction Kit version 3.1 according to manufacturer instructions. Sequencing was performed on an Illumina NovaSeq (S4) 300-cycle. Raw and processed data have been deposited in NCBI's GEO database (GSE291343).

scRNA-seq analysis, cluster identification, and gene marker determination

Data of each individual experiment was analyzed according to the following steps: Raw sequencing data was aligned to the mouse reference genome (GRCm39) and quantified using cellranger count (10× Genomics). The resulting count matrices were processed in R (version 4.3.1) using Seurat (version 5.0.1)[127]. Low-quality cells, defined as those exhibiting a high percentage of mitochondrial reads or a low number of detected features, were identified and removed using miQC[128] (version 1.10.0). Doublets were identified and removed using DoubletFinder (version 2.0.4)[129]. Datasets from individual experiments were merged and normalized using the SCTransform function from Seurat. To account for technical variability, we regressed out the percentage of reads mapped to mitochondria and ribosomal genes during normalization. We performed integration of the datasets using Harmony (version 1.2.0)[130]. Cell clusters were identified using the FindClusters function in Seurat using the Leiden algorithm (version 0.10.0)[131]. Uniform Manifold Approximation and Projection (UMAP) dimensional reduction was performed on the harmony-corrected embeddings using RunUMAP function in Seurat. Smoothed visualizations of gene expression in UMAP space was generated using Nebulosa (version 1.12.1), which employs kernel density estimates for enhanced visualization and interpretation[132]. Marker genes for each cluster were identified using the FindAllMarkers function in Seurat. Statistical significance was inferred using the Wilcoxon rank-sum test and adjusted for multiple testing using the Benjamini–Hochberg method. Cortical cell clusters (defined by the expression of cortical cell-specific marker Nr5a1) were further classified as ZG- or ZF-biased based on the expression of known ZG and ZF markers such as Vsnl1, Cyp11b2 (ZG), and Cyp11b1 (ZF). Grouped differential expression analysis between ZG- and ZF-biased clusters was performed using the FindMarkers function from Seurat. A volcano plot displaying the top 20 DEG genes was built using EnhancedVolcano (version 1.18.0). A CLOUPE file was generated from the Seurat-processed single cell gene expression dataset using the 10× Genomics' LoupeR (version 1.1.3) for interactive and visualization and exploration (see below Data availability).

Hormonal measurements

When hormone measurements were expected to be performed, mice were euthanized by decapitation in compliance with IACUC protocol between 8:30 and 10 am, within 30 s of handling to minimize stress-induced ACTH secretion. Core trunk blood was collected using sodium heparin-coated tubes (BD Vacutainer® Heparin Tubes, #367871) and centrifuged at 1800 × *g* for 20 min at 4 °C to obtain plasma. Samples were divided into two aliquots for ACTH and steroid measurements and stored at −80 °C prior to analysis. Corticosterone, Progesterone, 11-Deoxycorticosterone, and Testosterone concentration were determined by liquid chromatography-tandem mass spectrometry (LC-MS/MS).

Intra-adrenal cholesterol esters and free cholesterol measurement

For each mouse, both adrenals were harvested and placed in cold PBS 1×, removed fat and weighed for downstream calculation and homogenized in 600 µL of lipid extraction solution (Chloroform, Isopropanol, Igepal) as described by manufacturer (Abcam, #ab65359) with slight modifications. Adrenal tissues were homogenized using a BeadBug™ Microtube Homogenizer (2 × 30 s 400 (×10 speed)). Lysate was transferred into new 1.5 mL Eppendorf tubes and evaporated for 4 h at 50 °C in a chemical hood, then vacuum centrifuged for 30 min. Lipids were finally resuspended in 200 µL of assay buffer. Cholesterol levels were measured using two volumes that were preliminary determined to be in the range of the standard curve (5 and 10 µL for total cholesterol and 25 and 50 µL for Free cholesterol). The average quantity of cholesterol ester in *WT* adrenals was 9.6 µg/mg of adrenal gland, similar to published literature[133].

Ex vivo mouse adrenal explant culture

DHT stimulation: Seven-month-old female adrenals were quickly harvested after euthanasia and put in ice-cold PBS 1×. They were then cut in half under a tissue culture hood, in a tissue culture dish, using sterile single-edge razor blades (Persona GEM, #62-0179). In a 24-well plate (USA Scientific, #CC7682-7524), two half adrenals were placed in each well in 1 mL of DMEM/F-12 (GIBCO, #11330032) supplemented with 1% insulin-transferrin-selenium-ethanolamine (GIBCO, #51500056) and 1% Penicillin-Streptomycin (GIBCO, #15140122). No serum was added to avoid exogenous steroid contamination. After 24 h, explants were incubated with Vehicle or 5α-dihydrotestosterone (DHT) at 0.1 µM (Cerilliant, #D-073-1ML) for 48 h. RNA was extracted from explants using the Mini RNA extraction kit (RNeasy Mini Kit Qiagen, #74104). Dibutyryl cAMP stimulation (Bt2-cAMP): Dibutyryl-cAMP (sodium salt) (Sigma-Aldrich, #D0260 and Cell Signaling #35857) was resuspended in sterile water at a concentration of 0.1 mg/µL and used at a final concentration of 2.5 mM. After dissection, two half-adrenals were placed in each well in 1 mL of prewarmed DMEM/F-12 (GIBCO, #11330032) supplemented with 1% insulin-transferrin-selenium-ethanolamine (GIBCO, #51500056) and 1% Penicillin-Streptomycin (GIBCO, #15140122) for 1 h. No serum was added to avoid exogenous steroid contamination. Adrenals were then transferred into new wells and incubated with Vehicle (water) or Bt2-cAMP for the time indicated in the figures. Media was harvested at the end, and 2.5 µL of culture media was diluted 100 times in DMEM F12 and used for ELISA assays. Corticosterone levels (ENZO, #ADI-900-097) were assayed in duplicate according to manufacturer instructions. In this experiment, samples were not treated with the steroid displacement reagent.

Histology

Left adrenals were quickly transferred to be fixed in Formalin (FischerBrand, #427-098) for 24 h at room temperature under gentle agitation on an orbital shaker. The next day, adrenals were rinsed in PBS 1× for 10 min at room temperature and transferred in 70% ethanol until processing. Tissue processing was performed on a Leica ASP 300S Tissue Processor at the UMICH Orthopaedic Research Laboratories (ORL) Histology Core (15 min per station for adrenal, 1 h for larger tissues). Tissues were embedded in paraffin (Leica

Paraplast, #39601006), and 5 µm sections were obtained using a HistoCore BIOCUT microtome (Leica) on Superfrost™ Plus Microscope Slides (Fischer Scientific, #12-550-15). A minimum of two serial sections were placed on each slide, thus allowing the inclusion of negative controls for each biological replicate. Sections were first baked for 45 min-1 h in an incubator at 55 °C, then deparaffinized in histoclear (National Diagnostics, #HS-200) (2 times-5 min) and rehydrated in graded ethanol (2 times-5 min in absolute ethanol; 2 times-5 min in 95%; 1 time-5 min in 70%; 1 time-5 min in 50%). After 5 min under running tap water, slides were immersed in antigen retrieval according to the Supplementary Data 2. After 3 times-5 min washes in PBS 1×, slides were incubated in hydrogen peroxide (Sigma-Aldrich, #H1009, 0.3% v/v in water), for 30 min at room temperature to inhibit endogenous peroxidase. Hydrophobic barriers were drawn around each section with an ImmEdge pen (Vector Laboratories, #H-4000). After 3 times-5 min washes in PBS 1×, slides were blocked using 2.5%, ready to use, Horse or Goat Serum (Vector Laboratories, #S-2012-50, #S-1012-50) depending on the host specie of the secondary antibody. When antibody made in mouse was used, the M.O.M.® (Mouse on Mouse) ImmPRESS® HRP (Peroxidase) Polymer Kit (MP-2400) was used according to manufacturer instructions. Adrenal sections were then incubated overnight at 4 °C in a humid chamber with primary antibodies Supplementary Data 2. The following day, sections were rinsed 3 times-5 min in PBS 1× and incubated with appropriate secondary antibody (Vector Laboratories, Immpress HRP) for 30 or 10 min according to the manufacturer instructions (details in Supplementary Data 2). After 3 times-5 min washes in PBS 1×, staining was developed with ImmPACT® DAB EqV Substrate Kit, Peroxidase (HRP) (Vector Laboratories, #SK4103). Sections were then rinsed 3 times-5 min in PBS 1× and 1 time-5 min under running tap water. Hematoxylin staining (Sigma-Aldrich, #GHS132-1L) was then performed to visualize nuclei before mounting with Permount™ Mounting Medium. Images were acquired on a Nikon Optiphot-2 with an Olympus DP70 camera and the DP manager software (version 3.3.1.292). For PLIN1 quantification of integrated density, we used Fiji/ImageJ software (2.14.0/1.54 f/Java 1.8.0_66)[134,135] with the following parameters (Hue: 0–250, Saturation: 0–255, Brightness: 150–255, Thresholding method: Default, Threshold color: B&W, Color Space: HSB, Dark Background). For nuclear density, the adrenal cortex was divided into 3 equal tiers, and the number of nuclei was counted in each tier and divided by the area. Results are reported as number of nuclei per mm^2. Costaining. After HHEX staining was developed and sections rinsed 3 times-5 min in PBS 1×, slides were incubated in HCL 0.02 N in water for 20 min to inhibit peroxidase from the Immpress HRP secondary antibody. Sections were then rinsed 3 times-5 min in PBS 1× and blocked as described above, and incubated with DAB2 antibody overnight at 4 °C in a humid chamber. The following day, the secondary antibody was applied as described above, and staining was developed using the ImmPACT® VIP Substrate Kit, Peroxidase (HRP) (Vector Laboratories, #SK-4605). Visualization of endogenous fluorescence: All steps were performed using dark tube or foil-covered plates to minimize exposure to light. At dissection, left and right adrenals were quickly harvested, dissected from surrounding fat, and incubated for 2 h in 4% PFA at 4 °C, then incubated in Sucrose 30% (Sigma-Aldrich, #84097) diluted in PBS 1× overnight at 4 °C. The next day, adrenals were transferred into new tubes and incubated in Tissue-Plus™ O.C.T. Compound (Fisher Healthcare, #23-730-571) for 1 h at 4 °C. Finally, adrenals were transferred to cryomolds (Tissue-Tek, #4565) and embedded in O.C.T. on a dry ice ethanol bath. The blocks were stored at −80 °C until cryosection. The day of imaging, 5–7 µm thick sections were made on a cryostat (Leica CM 3050S) on Superfrost™ Plus Microscope Slides (Fischer Scientific, #12-550-15), incubated for 10 min in Hoechst (1:10 000 in PBS 1×) for nuclei visualization, then mounted in a PBS/glycerol 50% (v/v).

In situ single-molecule hybridization, RNAscope

Adrenals were fixed in 10% normal buffered formalin (VWR) for 24 h at room temperature, rinsed in PBS 1× for 10 min, and paraffin-embedded, and cut into 5 µm sections. The RNAscope™ 2.5 HD Reagent Kit-BROWN (Advanced Cell Diagnostics, #322300) was used according to the manufacturer's instructions. Probes are listed in Supplementary Data 2. Images were acquired on a Nikon Optiphot-2 with an Olympus DP70 camera.

In situ neutral lipid staining, Oil red O

Oil red O stock solution was prepared by adding 1.25 × *g* of ORO (Sigma-Aldrich, #00625) to 200 ml of 99% (vol/vol) isopropyl alcohol (Sigma-Aldrich, #I9516), and the solution was mixed with magnetic stirring for 2 h at room temperature. Snap-frozen adrenals were embedded in O.C.T. compound directly in mold in the cryostat's chamber. Organs were kept frozen during the entire process, and 5–7 µm thick sections were made on a cryostat (Leica CM 3050S) on Superfrost™ Plus Microscope Slides (Fischer Scientific, #12-550-15). Prior to storage at −80 °C, sections were dried at room temperature for 10 min to prevent detachment from the slides. Oil Red O working solution was prepared the day of the staining by adding 1.5 parts of ORO stock solution to one part of distilled water (30 ml of ORO to 20 ml of water). The solution was left at 4 °C for 10 min to thicken before filtration through a 45 µM filter (Corning, #430627) to remove precipitates. In the meantime, slides were equilibrated for 10 min at room temperature, then incubated for 5 min in Oil Red O working solution before being rinsed for 30 min with running tap water. The slides were finally mounted in PBS:Glycerol (Fischer chemical, #G33) solution (1:1), let sit for 10 min at room temperature and sealed using dots of Permount™ Mounting Medium on the edge of the coverslip (Corning, #2980-225).

RNA expression analysis

The right adrenals were quickly harvested after euthanasia, fat was quickly removed, and adrenal tissues were transferred into a tube, snap frozen, and stored at −80 °C. At the time of RNA extraction, each adrenal was quickly transferred into a Lysing Matrix D 2 mL tube (MP Biochemicals, #6913100) containing 600 µL of RLT lysis Buffer (RNeasy Mini Kit Qiagen, 74104) supplemented with 6 µL of 2-mercaptoethanol (Sigma-Aldrich, M7522). Lysis was performed using a BeadBug™ Microtube Homogenizer (2 × 30 s 400 (×10 speed)). Lysat was transferred into new 1.5 mL tubes and an equal volume of 70% ethanol was added and mixed by pipetting. RNA was extracted according to manufacturer instructions with few modifications as follow to avoid contamination with Thiocyanate Guanidine in the final eluted sample. New collection tubes were used after each step of centrifugation so that the exterior of the column never came in contact with previously discarded flowthrough. Additional collection tubes were made by cutting the lids of 2 mL centrifuge tubes (USA Scientific, #1620-2700). An additional step of centrifugation was added after the RW1 step to ensure complete removal from the column. When rinsing the column with 500 µL of RPE, the inside of the lid and the inner wall from the top of the column were rinsed during both washes. An additional centrifugation step was performed for 1 min at full speed (12,000 × *g*) to completely dry the membrane before elution. RNAs from male adrenals were eluted in 20 µL of water and 30 µL for female adrenals. RNA quality and concentration were assessed using a nanodrop (expected 260/280 ratio >1.8 and 260/230 ratio 2-2.2). RNAs were then stored at −80 °C until retrotranscription or library preparation for RNAseq. For RT-qPCR, 500 ng of RNA were treated with DNAse (Invitrogen, #18068-015) according to manufacturer instructions, and retrotranscribed into cDNAs at a final volume of 20 µL using the High-Capacity cDNA Reverse Transcription Kit (Applied Biosystems, #4368814). cDNAs were diluted 10 times in water, and 2 µL were used for qPCR, which was performed in MicroAmp Endura Plate Optical 96

well fast clear (Applied Biosystems, # 4483485), using the Power SYBR Green PCR Master Mix (Applied Biosystems, # 4367659) in a final volume of 10 µL. Relative gene expression was determined using the ΔΔCt method using *Actb* (Actin beta) as a housekeeping gene and averaging duplicates for each biological replicates. Primer pairs are listed in Supplementary Data 2. Adrenal gene expression profiles for four 6-week-old *Sf1-Cre^{high}; Hhex$^{flox/flox}$* and four *WT* littermates were analyzed by bulk RNA sequencing. RNA samples were similarly treated with DNAse, and quality was evaluated by Bioanalyzer 2100 (Eukaryote Total RNA Nano chip, Agilent) at the Advanced Genomic Core at the University of Michigan (RIN > = 7.50 and free of genomic DNA contamination). Libraries were prepared from total RNA using standard poly(A) capture-based protocols and sequenced in paired-end mode on a NovaSeq (S4) 300. Sequencing quality metrics, including base quality scores and read count, were assessed using FastQC. Adapter sequences and low-quality bases were trimmed using the bbduk tool from BBTools. Processed paired-end reads were aligned to the mouse transcriptome sequence (GENCODE release M28, obtained from https://www.gencodegenes.org) using Kallisto[136]. Transcript-level abundance estimates were summarized to gene-level expression values using the lengthScaledTPM method in tximport[137]. Downstream analyses were performed in R using Bioconductor packages. To account for differences in library size, gene-level expression data were normalized using the Trimmed Mean of M-values (TMM) method implemented in edgeR[138]. Lowly expressed genes were filtered out using the filterByExpr function from edgeR to retain only genes with biologically meaningful expression levels. Unwanted and hidden sources of variation, such as batch effects, were removed using the sva package[139]. PCA was performed using the standard prcomp function in R, and biplots were constructed using ggplot2. Differential gene expression analysis was performed using limma[140]. Raw and processed data have been deposited in NCBI's GEO database (GSE291472). Common differentially expressed genes between 6-week-old male *Sf1-Cre^{high} Hhex KO* compared to their respective littermate *WT* and 25-week-old male ARKO compared to their respective littermate *WT* are available in Supplementary Data 1.

Genome-wide profiling of DNA-binding proteins, cleavage under targets and tagmentation (CUT&Tag-IT™)

CUT&Tag-IT™ Assay Kit–Tissue (Active Motif, #53170) was used according to manufacturer instructions. Briefly, fresh adrenals from 6 to 9-week-old *WT* males were quickly harvested after euthanasia, cleaned from fat and transferred into ice-cold PBS 1× until being weighed. 10 mg of tissue (4 to 6 adrenals) was used for nuclei preparation, including the following conditions: no primary antibody, H3K27ac, and AR. For each condition, 20 µL of concanavalin A beads were prepared at room temperature according to manufacturer instructions. Briefly, 10 mg of tissue was lysed in 1 mL of Lysis buffer, and nuclei were extracted using a 1 mL dounce homogenizer. Lysate was filtered through 40 µm strainer, and nuclei were pelleted by centrifugation at 4 °C. A range of 127000–170000 nuclei per mg of male mouse adrenals were obtained, and 280000 nuclei per conditions were used. Nuclei were then bound to concanavalin A beads and incubated at 4 °C overnight with primary antibodies (Supplementary Data 2). The following day, guinea pig anti-rabbit secondary antibody was bound to primary antibodies, followed by an incubation with assembled pA-Tn5 transposomes. Tagmentation was then achieved by incubating samples at 37 °C for 1 h. DNA was then solubilized, purified, and eluted. 30 µL of tagmented DNA was used to prepare libraries. Libraries were sequentially purified using SPRI Bead clean up from the kit, and AMPure XP Reagent (Beckman Coulter, #A63880) according to the manufacturer's instructions. The quality of the library was assessed on a Bioanalyser at the Advanced Genomic Core at the University of Michigan. Libraries were sequenced on an Illumina NextSeq 500 platform using the P1 100-cycle kit in paired-end mode. Raw sequencing reads were processed using the following bioinformatics pipeline. Read preprocessing: Paired-end reads were interleaved using seqtk merge (https://github.com/lh3/seqtk). Adapter sequences and low-quality bases were trimmed using fastp (https://github.com/OpenGene/fastp) with default parameters. Quality control reports, including read length distribution, base quality, and adapter content, were generated in HTML format. Alignment: Preprocessed reads were aligned to the mm10 mouse reference genome using Bowtie2 (version 2.3.5.1) with the following parameters: –local –very-sensitive –no-mixed –no-discordant -I 10 -X 700 to ensure high sensitivity for local alignment while preventing discordant and mixed alignments. Peak calling: Peaks were called using Genrich (https://github.com/jsh58/Genrich), with the -j option to enable ATAC-seq mode, which adjust for the insertion bias caused by the Tn5 transposase. To visualize genome-wide signal distributions, BigWig files were generated from the aligned BAM files using the bam_to_bigwig function from the GenomicAlignments package in R. Signal to noise was assessed by calculating the Fraction of Reads in Peaks (FRiP) and the TSS enrichment score. For H3K27ac, the FRiP score was 39% and the TSS enrichment score was 11.34231. For AR, the FriP score was 15% and the TSS enrichment score was 12.92894. Raw and processed data have been deposited in NCBI's GEO database (GSE291344).

Software and applications

Graphs were generated using GraphPad Prism (10.2.2). Illustrations and Figures were created using PowerPoint (Version 2411 Build 16.0.18277.20082), the free life science icon library from Biorender.com, and R for the UMAP, the Inferno plots and the Volcano plot. The plugin Grammarly for Microsoft Word was used for grammar and spell-checking purposes at writing and editing stages of the manuscript. Literature references were added using the Zotero app (7.0.13).

Statistics, scientific rigor, and reproducibility

GraphPad Prism (10.2.2), R (version 4.3.1), and G*Power (Version 3.1.9.7) were used for statistical analysis. Details related to the statistical test, number of biological replicates, mean, standard deviation, *t*-values, degree of freedom, *F*-value, power, and *p*-value are available in Source Data and Supplementary Data 3. No data was excluded from the analyses. A p-value < 0.05 was considered significant. Exact p-values of interest are reported on each graphs together with appropriate star symbols (* < 0.05, **<0.01, *** <0.001, **** <0.0001). When comparing two independent groups, we assessed the normality of the data by performing a Shapiro–Wilk test. If passed, a two-tailed unpaired *t*-test was performed to compare the means with a Welch correction to address issues related to unequal variances (F value ≠ 1), and differences in sample size between groups. When data were not passing the normality test, a two-tailed Mann–Whitney test was applied to compare the ranks. Sample size was determined based on preliminary data and power calculations performed using G*Power to obtain >80% power with 5% type 1 error. When the p-value was <0.05, but 80% power could not be reached, an orthogonal approach was employed (detailed in Supplementary Data 3). For more than two-groups, we performed a two-way or three-way ANOVA, followed by a Šídák's multiple comparisons test. For histology, samples were blinded before analysis. When possible, orthogonal methods were used to ensure reproducibility of the results. For example, genes of interest identified by scRNAseq and bulk RNAseq were confirmed by RT-qPCR and/or immunohistochemistry on larger cohorts.

Nomenclature

Gene symbols were italicized, with only the first letter in upper-case for mouse species. Protein symbols were set in roman type, and all letters in upper case according to the following resources, https://www.genenames.org and https://www.informatics.jax.org.

Ethical approval declaration

All experiments were carried out in accordance with protocols approved by the Institutional Animal Care & Use Committee (IACUC) at the University of Michigan (protocol #00010217), the guidelines set by the National Institutes of Health (NIH), and the three R rule (Replacement, Reduction, and Refinement). All efforts were made to minimize animal suffering and distress.

Reporting summary

Further information on research design is available in the Nature Portfolio Reporting Summary linked to this article.

Data availability

All sequencing datasets generated in this study have been deposited in the Gene Expression Omnibus (GEO) database under the accession code GSE291343, GSE291472, and GSE291344. Processed data are provided in Supplementary Data 1. The CLOUPE file related to the scRNAseq dataset presented in this manuscript is accessible at the following address [https://doi.org/10.6084/m9.figshare.28612406]. Source data are provided with this paper.

References

1. Kuo, T., McQueen, A., Chen, T.-C. & Wang, J.-C. Regulation of glucose homeostasis by glucocorticoids. *Adv. Exp. Med. Biol.* **872**, 99–126 (2015).
2. Cain, D. W. & Cidlowski, J. A. Immune regulation by glucocorticoids. *Nat. Rev. Immunol.* **17**, 233–247 (2017).
3. Dickmeis, T. Glucocorticoids and the circadian clock. *J. Endocrinol.* **200**, 3–22 (2009).
4. Marin, M.-F. et al. Chronic stress, cognitive functioning and mental health. *Neurobiol. Learn. Mem.* **96**, 583–595 (2011).
5. Shimba, A. & Ikuta, K. Glucocorticoids regulate circadian rhythm of innate and adaptive immunity. *Front. Immunol.* **11**, 2143 (2020).
6. Lacroix, A. Cardiometabolic morbidity of mild cortisol excess. *Ann. Intern. Med.* https://doi.org/10.7326/M21-4526 (2022).
7. Mitani, F. et al. Cytochrome P-45011 beta and P-450scc in adrenal cortex: zonal distribution and intramitochondrial localization by the horseradish peroxidase-labeled antibody method. *J. Histochem. Cytochem.* **30**, 1066–1074 (1982).
8. Sugano, S. et al. Monoclonal antibodies against bovine adrenal cytochrome P-450(11 beta) and cytochrome P-450SCC. Their isolation, characterization and application to immunohistochemical analysis of adrenal cortex. *J. Steroid Biochem.* **23**, 1013–1021 (1985).
9. Ogishima, T., Suzuki, H., Hata, J., Mitani, F. & Ishimura, Y. Zone-specific expression of aldosterone synthase cytochrome P-450 and cytochrome P-45011 beta in rat adrenal cortex: histochemical basis for the functional zonation. *Endocrinology* **130**, 2971–2977 (1992).
10. Ho, M. M. & Vinson, G. P. 11 beta-hydroxylase gene expression in the rat adrenal cortex. *J. Endocrinol.* **139**, 301–306 (1993).
11. Erdmann, B., Denner, K., Gerst, H., Lenz, D. & Bernhardt, R. Human adrenal CYP11B1: localization by in situ-hybridization and functional expression in cell cultures. *Endocr. Res.* **21**, 425–435 (1995).
12. Gomez-Sanchez, C. E. et al. Development of monoclonal antibodies against human CYP11B1 and CYP11B2. *Mol. Cell. Endocrinol.* **383**, 111–117 (2014).
13. Arakane, F. et al. Phosphorylation of steroidogenic acute regulatory protein (StAR) modulates its steroidogenic activity. *J. Biol. Chem.* **272**, 32656–32662 (1997).
14. Clark, B. J. et al. Hormonal and developmental regulation of the steroidogenic acute regulatory protein. *Mol. Endocrinol. Baltim. Md* **9**, 1346–1355 (1995).
15. Lopez, J. P. et al. Single-cell molecular profiling of all three components of the HPA axis reveals adrenal ABCB1 as a regulator of stress adaptation. *Sci. Adv.* **7**, eabe4497 (2021).
16. Lerario, A. M., Mohan, D. R. & Hammer, G. D. Update on biology and genomics of adrenocortical carcinomas: rationale for emerging therapies. *Endocr. Rev.* **43**, 1051–1073 (2022).
17. Paz, H., Lynch, M. R., Bogue, C. W. & Gasson, J. C. The homeobox gene Hhex regulates the earliest stages of definitive hematopoiesis. *Blood* **116**, 1254–1262 (2010).
18. Guiral, M., Bess, K., Goodwin, G. & Jayaraman, P. S. PRH represses transcription in hematopoietic cells by at least two independent mechanisms. *J. Biol. Chem.* **276**, 2961–2970 (2001).
19. Swingler, T. E., Bess, K. L., Yao, J., Stifani, S. & Jayaraman, P.-S. The proline-rich homeodomain protein recruits members of the Groucho/Transducin-like enhancer of split protein family to co-repress transcription in hematopoietic cells. *J. Biol. Chem.* **279**, 34938–34947 (2004).
20. Yang, D. et al. CRISPR screening uncovers a central requirement for HHEX in pancreatic lineage commitment and plasticity restriction. *Nat. Cell Biol.* **24**, 1064–1076 (2022).
21. Bort, R. Hex homeobox gene-dependent tissue positioning is required for organogenesis of the ventral pancreas. *Development* **131**, 797–806 (2004).
22. Bort, R., Signore, M., Tremblay, K., Barbera, J. P. M. & Zaret, K. S. Hex homeobox gene controls the transition of the endoderm to a pseudostratified, cell emergent epithelium for liver bud development. *Dev. Biol.* **290**, 44–56 (2006).
23. Keng, V. W. et al. Homeobox gene hex is essential for onset of mouse embryonic liver development and differentiation of the monocyte lineage. *Biochem. Biophys. Res. Commun.* **276**, 1155–1161 (2000).
24. Martinez Barbera, J. P. et al. The homeobox gene Hex is required in definitive endodermal tissues for normal forebrain, liver and thyroid formation. *Dev. Camb. Engl.* **127**, 2433–2445 (2000).
25. Zhang, J., McKenna, L. B., Bogue, C. W. & Kaestner, K. H. The diabetes gene Hhex maintains -cell differentiation and islet function. *Genes Dev.* **28**, 829–834 (2014).
26. Alfaifi, M. Contribution of genetic variant identified in HHEX gene in the overweight Saudi patients confirmed with type 2 diabetes mellitus. *Saudi J. Biol. Sci.* **29**, 804–808 (2022).
27. Wang, X. et al. The association between HHEX single-nucleotide polymorphism rs5015480 and gestational diabetes mellitus: a meta-analysis. *Medicine (Baltimore)* **99**, e19478 (2020).
28. Li, C. et al. Association between single nucleotide polymorphisms in CDKAL1 and HHEX and type 2 diabetes in Chinese population. *Diabetes Metab. Syndr. Obes. Targets Ther.* **13**, 5113–5123 (2020).
29. Ragvin, A. et al. Long-range gene regulation links genomic type 2 diabetes and obesity risk regions to HHEX, SOX4, and IRX3. *Proc. Natl. Acad. Sci. USA* **107**, 775–780 (2010).
30. Sladek, R. et al. A genome-wide association study identifies novel risk loci for type 2 diabetes. *Nature* **445**, 881–885 (2007).
31. Cauchi, S. et al. Post genome-wide association studies of novel genes associated with type 2 diabetes show gene-gene interaction and high predictive value. *PLoS ONE* **3**, e2031 (2008).
32. van Vliet-Ostaptchouk, J. V. et al. HHEX gene polymorphisms are associated with type 2 diabetes in the Dutch Breda cohort. *Eur. J. Hum. Genet.* **16**, 652–656 (2008).
33. Chiang, C.-W., Chou, Y.-H., Huang, C.-N., Lu, W.-Y. & Liaw, Y.-P. Gender-specific genetic influence of rs1111875 on diabetes risk: insights from the Taiwan biobank study. *J. Diabetes Investig.* https://doi.org/10.1111/jdi.14359 (2024).
34. Zhai, G. et al. Eight common genetic variants associated with serum DHEAS levels suggest a key role in ageing mechanisms. *PLoS Genet.* **7**, e1002025 (2011).

35. Vernerova, L. et al. Contribution of genetic factors to lower DHEAS in patients with rheumatoid arthritis. *Cell. Mol. Neurobiol.* **38**, 379–383 (2018).
36. Kaya-Okur, H. S. et al. CUT&Tag for efficient epigenomic profiling of small samples and single cells. *Nat. Commun.* **10**, 1930 (2019).
37. Bingham, N. C., Verma-Kurvari, S., Parada, L. F. & Parker, K. L. Development of a steroidogenic factor 1/Cre transgenic mouse line. *Genes* **44**, 419–424 (2006).
38. Muzumdar, M. D., Tasic, B., Miyamichi, K., Li, L. & Luo, L. A global double-fluorescent Cre reporter mouse. *Genesis* **45**, 593–605 (2007).
39. Basham, K. J. et al. A ZNRF3-dependent Wnt/β-catenin signaling gradient is required for adrenal homeostasis. *Genes Dev.* **33**, 209–220 (2019).
40. Mathieu, M. et al. Steroidogenic differentiation and PKA signaling are programmed by histone methyltransferase EZH2 in the adrenal cortex. *Proc. Natl. Acad. Sci. USA* **115**, E12265–E12274 (2018).
41. Dufour, D. et al. Loss of SUMO-specific protease 2 causes isolated glucocorticoid deficiency by blocking adrenal cortex zonal transdifferentiation in mice. *Nat. Commun.* **13**, 7858 (2022).
42. Gjerstad, J. K., Lightman, S. L. & Spiga, F. Role of glucocorticoid negative feedback in the regulation of HPA axis pulsatility. *Stress* **21**, 403–416 (2018).
43. Ramamoorthy, S. & Cidlowski, J. A. Corticosteroids. *Rheum. Dis. Clin. N. Am.* **42**, 15–31 (2016).
44. Holst, J. P., Soldin, O. P., Guo, T. & Soldin, S. J. Steroid hormones: relevance and measurement in the clinical laboratory. *Clin. Lab. Med.* **24**, 105–118 (2004).
45. Rosol, T. J. & Gröne, A. Chapter 3 - Endocrine glands. In *Jubb, Kennedy & Palmer's Pathology of Domestic Animals: Volume 3 (Sixth Edition)* (ed. Maxie, M. G.) 269–357.e1 (W.B. Saunders, 2016).
46. Acconcia, F. & Marino, M. Steroid hormones: synthesis, secretion, and transport. In *Principles of Endocrinology and Hormone Action* (eds Belfiore, A. & LeRoith, D.) 43–72 (Springer International Publishing, Cham, 2018).
47. Lightman, S. L., Birnie, M. T. & Conway-Campbell, B. L. Dynamics of ACTH and cortisol secretion and implications for disease. *Endocr. Rev.* **41**, bnaa002 (2020).
48. Dailey, R. E., Swell, L. & Treadwell, C. R. Utilization of free and esterified gholesterol-4-G14 for corticoid biosynthesis by hog adrenal homogenates. *Proc. Soc. Exp. Biol. Med.* **110**, 571–574 (1962).
49. Long, C. N. H. The relation of cholesterol and ascorbic acid to the secretion of the adrenal cortex. *Recent Prog. Horm. Res.* **1**, 99–122 (1947).
50. Wang, N., Wang, W., Breslow, J. L. & Tall, A. R. Scavenger receptor BI (SR-BI) is up-regulated in adrenal gland in apolipoprotein A-I and hepatic lipase knock-out mice as a response to depletion of cholesterol stores. In vivo evidence that SR-BI is a functional high density lipoprotein receptor under feedback control. *J. Biol. Chem.* **271**, 21001–21004 (1996).
51. Shroff, A. & Nazarko, T. Y. SQSTM1, lipid droplets and current state of their lipophagy affairs. *Autophagy* **19**, 720–723 (2023).
52. Wang, L. et al. Ethanol-triggered lipophagy requires SQSTM1 in AML12 hepatic cells. *Sci. Rep.* **7**, 12307 (2017).
53. Kumar, A. V., Mills, J. & Lapierre, L. R. Selective autophagy receptor p62/SQSTM1, a pivotal player in stress and aging. *Front. Cell Dev. Biol.* **10**, 793328 (2022).
54. Mizushima, N., Yoshimori, T. & Levine, B. Methods in mammalian autophagy research. *Cell* **140**, 313–326 (2010).
55. Freedman, B. D. et al. Adrenocortical zonation results from lineage conversion of differentiated zona glomerulosa cells. *Dev. Cell* **26**, 666–673 (2013).
56. Pihlajoki, M. et al. Conditional mutagenesis of Gata6 in SF1-positive cells causes gonadal-like differentiation in the adrenal cortex of mice. *Endocrinology* https://doi.org/10.1210/en.2012-1892 (2013).
57. Mauthe, M. et al. Chloroquine inhibits autophagic flux by decreasing autophagosome-lysosome fusion. *Autophagy* **14**, 1435–1455 (2018).
58. Beyer, C. & Komisaruk, B. Effects of diverse androgens on estrous behavior, lordosis reflex, and genital tract morphology in the rat. *Horm. Behav.* **2**, 217–225 (1971).
59. Brown-Grant, K., Munck, A., Naftolin, F. & Sherwood, M. R. The effects of the administration of testosterone propionate alone or with phenobarbitone and of testosterone metabolites to neonatal female rats. *Horm. Behav.* **2**, 173–182 (1971).
60. De Gendt, K. et al. A Sertoli cell-selective knockout of the androgen receptor causes spermatogenic arrest in meiosis. *Proc. Natl. Acad. Sci. USA.* **101**, 1327–1332 (2004).
61. Nikkanen, J. et al. An evolutionary trade-off between host immunity and metabolism drives fatty liver in male mice. *Science* **378**, 290–295 (2022).
62. Jo, S. et al. Sex differences in pancreatic β-cell physiology and glucose homeostasis in C57BL/6J mice. *J. Endocr. Soc.* **7**, bvad099 (2023).
63. Dumontet, T. et al. PKA signaling drives reticularis differentiation and sexually dimorphic adrenal cortex renewal. *JCI Insight* **3**, e98394 (2018).
64. Grabek, A. et al. The adult adrenal cortex undergoes rapid tissue renewal in a sex-specific manner. *Cell Stem Cell* **25**, 290–296.e2 (2019).
65. Levasseur, A., Dumontet, T. & Martinez, A. "Sexual dimorphism in adrenal gland development and tumorigenesis". *Curr. Opin. Endocr. Metab. Res.* **8**, 60–65 (2019).
66. Yeung, K. Y. & Ruzzo, W. L. Principal component analysis for clustering gene expression data. *Bioinforma. Oxf. Engl.* **17**, 763–774 (2001).
67. Lyu, Q. et al. RNA-seq reveals sub-zones in mouse adrenal zona fasciculata and the sexually dimorphic responses to thyroid hormone. *Endocrinology* **161**, bqaa126 (2020).
68. Wakil, A. E., Mari, B., Barhanin, J. & Lalli, E. Genomic analysis of sexual dimorphism of gene expression in the mouse adrenal gland. *Horm. Metab. Res.* **45**, 870–873 (2013).
69. Mukai, T. et al. Sexually dimorphic expression of Dax-1 in the adrenal cortex. *Genes Cells Devoted Mol. Cell. Mech.* **7**, 717–729 (2002).
70. Devine, K. et al. The ATP-binding cassette proteins ABCB1 and ABCC1 as modulators of glucocorticoid action. *Nat. Rev. Endocrinol.* **19**, 112–124 (2023).
71. Menzies, R. I. et al. Transcription controls growth, cell kinetics and cholesterol supply to sustain ACTH responses. *Endocr. Connect.* **6**, 446–457 (2017).
72. Vogel, F. et al. Polymorphism in the drug transporter gene ABCB1 as a potential disease modifier in cortisol-producing adrenal adenomas. *Exp. Clin. Endocrinol. Diabetes* **132**, 608–613 (2024).
73. Hammer, G. D. & Basham, K. J. Stem cell function and plasticity in the normal physiology of the adrenal cortex. *Mol. Cell. Endocrinol.* **519**, 111043 (2021).
74. Guasti, L., Paul, A., Laufer, E. & King, P. Localization of Sonic hedgehog secreting and receiving cells in the developing and adult rat adrenal cortex. *Mol. Cell. Endocrinol.* **336**, 117–122 (2011).
75. Neirijnck, Y. et al. Single-cell transcriptomic profiling redefines the origin and specification of early adrenogonadal progenitors. *Cell Rep.* **42**, 112191 (2023).

76. Pivovarova, O., Nikiforova, V. J., Pfeiffer, A. F. H. & Rudovich, N. The influence of genetic variations in HHEX gene on insulin metabolism in the German MESYBEPO cohort. *Diabetes Metab. Res. Rev.* **25**, 156–162 (2009).
77. Staiger, H. et al. A candidate type 2 diabetes polymorphism near the HHEX locus affects acute glucose-stimulated insulin release in European populations: results from the EUGENE2 study. *Diabetes* **57**, 514–517 (2008).
78. Pascoe, L. et al. Common variants of the novel type 2 diabetes genes CDKAL1 and HHEX/IDE are associated with decreased pancreatic beta-cell function. *Diabetes* **56**, 3101–3104 (2007).
79. Grarup, N. et al. Studies of association of variants near the HHEX, CDKN2A/B, and IGF2BP2 genes with type 2 diabetes and impaired insulin release in 10,705 danish subjects: validation and extension of genome-wide association studies. *Diabetes* **56**, 3105–3111 (2007).
80. Liu, S. et al. Genetic variants at 10q23.33 are associated with plasma lipid levels in a Chinese population. *J. Biomed. Res.* **28**, 53–58 (2014).
81. Dumontet, T. & Martinez, A. Adrenal androgens, adrenarche, and zona reticularis: a human affair? *Mol. Cell. Endocrinol.* **528**, 111239 (2021).
82. Kraemer, F. B. et al. Adrenal neutral cholesteryl ester hydrolase: identification, subcellular distribution, and sex differences. *Endocrinology* **143**, 801–806 (2002).
83. Li, H. et al. Hormone-sensitive lipase deficiency in mice causes lipid storage in the adrenal cortex and impaired corticosterone response to corticotropin stimulation. *Endocrinology* **143**, 3333–3340 (2002).
84. Al, E. M. et al. Wolman's disease: the king faisal specialist hospital and research centre experience. *Ann. Saudi Med.* **18**, 120–124 (1998).
85. Perry, R. et al. Primary adrenal insufficiency in children: twenty years experience at the Sainte-Justine Hospital, Montreal. *J. Clin. Endocrinol. Metab.* **90**, 3243–3250 (2005).
86. Menon, J. et al. Wolman's disease: a rare cause of infantile cholestasis and cirrhosis. *J. Pediatr. Genet.* **11**, 132–134 (2020).
87. Foladi, N. & Aien, M. T. CT features of Wolman disease (lysosomal acid lipase enzyme deficiency) – A case report. *Radiol. Case Rep.* **16**, 2857–2861 (2021).
88. Sen, D., Satija, L., Saxena, S., Rastogi, V. & Singh, M. A rare constellation of imaging findings in Wolman disease. *Med. J. Armed Forces India* **71**, S448–S451 (2015).
89. Fulcher, A. S., Das Narla, L. & Hingsbergen, E. A. Pediatric case of the day. Wolman disease (primary familial xanthomatosis with involvement and calcification of the adrenal glands). *RadioGraphics* **18**, 533–535 (1998).
90. Wolman, M., Sterk, V. V., Gatt, S. & Frenkel, M. Primary familial xanthomatosis with involvement and calcification of the adrenals. Report of two more cases in siblings of a previously described infant. *Pediatrics* **28**, 742–757 (1961).
91. Abramov, A., Schorr, S. & Wolman, M. Generalized xanthomatosis with calcified adrenals. *AMA J. Dis. Child.* **91**, 282–286 (1956).
92. Low, G., Irwin, G. J., MacPhee, G. B. & Robinson, P. H. Characteristic imaging findings in Wolman's disease. *Clin. Radiol. Extra* **59**, 106–108 (2004).
93. Schaub, J. et al. Wolman's disease: clinical, biochemical and ultrastructural studies in an unusual case without striking adrenal calcification. *Eur. J. Pediatr.* **135**, 45–53 (1980).
94. Zhang, S. et al. The regulation, function, and role of lipophagy, a form of selective autophagy, in metabolic disorders. *Cell Death Dis.* **13**, 1–11 (2022).
95. Gao, F. et al. Autophagy regulates testosterone synthesis by facilitating cholesterol uptake in Leydig cells. *J. Cell Biol.* **217**, 2103–2119 (2018).
96. Ma, Y. et al. Lipophagy contributes to testosterone biosynthesis in male rat leydig cells. *Endocrinology* **159**, 1119–1129 (2018).
97. Esmaeilian, Y. et al. Autophagy regulates sex steroid hormone synthesis through lysosomal degradation of lipid droplets in human ovary and testis. *Cell Death Dis.* **14**, 1–13 (2023).
98. Berruti, A. et al. Prognostic role of overt hypercortisolism in completely operated patients with adrenocortical cancer. *Eur. Urol.* **65**, 832–838 (2014).
99. Vanbrabant, T., Fassnacht, M., Assie, G. & Dekkers, O. M. Influence of hormonal functional status on survival in adrenocortical carcinoma: systematic review and meta-analysis. *Eur. J. Endocrinol.* **179**, 429–436 (2018).
100. Jeong, S.-J. et al. Prdx1 (peroxiredoxin 1) deficiency reduces cholesterol efflux via impaired macrophage lipophagic flux. *Autophagy* **14**, 120–133 (2018).
101. Chen, K., Yuan, R., Zhang, Y., Geng, S. & Li, L. Tollip deficiency alters atherosclerosis and steatosis by disrupting lipophagy. *J. Am. Heart Assoc.* **6**, e004078 (2017).
102. Ouimet, M. et al. microRNA-33 regulates macrophage autophagy in atherosclerosis. *Arterioscler. Thromb. Vasc. Biol.* **37**, 1058–1067 (2017).
103. Carotti, S. et al. Lipophagy impairment is associated with disease progression in NAFLD. *Front. Physiol.* **11**, 850 (2020).
104. Fu, Y. et al. Degradation of lipid droplets by chimeric autophagy-tethering compounds. *Cell Res.* **31**, 965–979 (2021).
105. Minami, Y. et al. Liver lipophagy ameliorates nonalcoholic steatohepatitis through extracellular lipid secretion. *Nat. Commun.* **14**, 4084 (2023).
106. Müller, M. B. et al. ABCB1 (MDR1)-type P-glycoproteins at the blood-brain barrier modulate the activity of the hypothalamic-pituitary-adrenocortical system: implications for affective disorder. *Neuropsychopharmacology* **28**, 1991–1999 (2003).
107. Flynn, S. D. et al. P-glycoprotein expression and multidrug resistance in adrenocortical carcinoma. *Surgery* **112**, 981–986 (1992).
108. Creemers, S. G. et al. MDR1 inhibition increases sensitivity to doxorubicin and etoposide in adrenocortical cancer. *Endocr. Relat. Cancer* **26**, 367–378 (2019).
109. Bechmann, N. et al. Asymmetric adrenals: sexual dimorphism of adrenal tumors. *J. Clin. Endocrinol. Metab.* **109**, 471–482 (2024).
110. Takahashi, F. et al. Development of sexual dimorphism of skeletal muscles through the adrenal cortex, caused by androgen-induced global gene suppression. *Cell Rep.* **43**, 113715 (2024).
111. Wilson, S., Qi, J. & Filipp, F. V. Refinement of the androgen response element based on ChIP-Seq in androgen-insensitive and androgen-responsive prostate cancer cell lines. *Sci. Rep.* **6**, 32611 (2016).
112. Hunter, M. P. et al. The homeobox gene Hhex is essential for proper hepatoblast differentiation and bile duct morphogenesis. *Dev. Biol.* **308**, 355–367 (2007).
113. Ferreira, M. J. et al. Spontaneous pancreatitis caused by tissue-specific gene ablation of Hhex in mice. *Cell. Mol. Gastroenterol. Hepatol.* **1**, 550–569 (2015).
114. Watanabe, H. et al. Transcription factor hematopoietically expressed homeobox protein (Hhex) negatively regulates osteoclast differentiation by controlling cyclin-dependent kinase inhibitors. *JBMR Plus* **6**, e10608 (2022).
115. Jackson, J. T. et al. A crucial role for the homeodomain transcription factor Hhex in lymphopoiesis. *Blood* **125**, 803–814 (2015).
116. Kim, A. C. et al. Targeted disruption of β-catenin in Sf1-expressing cells impairs development and maintenance of the adrenal cortex. *Development* **135**, 2593–2602 (2008).

117. King, P., Paul, A. & Laufer, E. Shh signaling regulates adrenocortical development and identifies progenitors of steroidogenic lineages. *Proc. Natl. Acad. Sci. USA* **106**, 21185–21190 (2009).
118. Huang, C.-C. J. & Yao, H. H. Inactivation of Dicer1 in Steroidogenic factor 1-positive cells reveals tissue-specific requirement for Dicer1 in adrenal, testis, and ovary. *BMC Dev. Biol.* **10**, 66 (2010).
119. Tevosian, S. G. et al. Adrenal development in mice requires GATA4 and GATA6 transcription factors. *Endocrinology* **156**, 2503–2517 (2015).
120. Drelon, C. et al. PKA inhibits WNT signalling in adrenal cortex zonation and prevents malignant tumour development. *Nat. Commun.* **7**, 12751 (2016).
121. Vidal, V. et al. The adrenal capsule is a signaling center controlling cell renewal and zonation through Rspo3. *Genes Dev.* **30**, 1389–1394 (2016).
122. Dumontet, T. et al. Hormonal and spatial control of SUMOylation in the human and mouse adrenal cortex. *FASEB J.* **33**, 10218–10230 (2019).
123. Heaton, J. H. et al. Progression to adrenocortical tumorigenesis in mice and humans through insulin-like growth factor 2 and β-catenin. *Am. J. Pathol.* **181**, 1017–1033 (2012).
124. Krill, K. T., Gurdziel, K., Heaton, J. H., Simon, D. P. & Hammer, G. D. Dicer deficiency reveals microRNAs predicted to control gene expression in the developing adrenal cortex. *Mol. Endocrinol.* **27**, 754–768 (2013).
125. Ching, S. & Vilain, E. Targeted disruption of Sonic Hedgehog in the mouse adrenal leads to adrenocortical hypoplasia. *Genesis* **47**, 628–637 (2009).
126. Truett, G. E. et al. Preparation of PCR-quality mouse genomic DNA with hot sodium hydroxide and tris (HotSHOT). *BioTechniques* **29**, 52 (2000).
127. Hao, Y. et al. Dictionary learning for integrative, multimodal and scalable single-cell analysis. *Nat. Biotechnol.* **42**, 293–304 (2024).
128. Hippen, A. A. et al. miQC: an adaptive probabilistic framework for quality control of single-cell RNA-sequencing data. *PLoS Comput. Biol.* **17**, e1009290 (2021).
129. McGinnis, C. S., Murrow, L. M. & Gartner, Z. J. DoubletFinder: doublet detection in single-cell RNA sequencing data using artificial nearest neighbors. *Cell Syst.* **8**, 329–337.e4 (2019).
130. Korsunsky, I. et al. Fast, sensitive and accurate integration of single-cell data with Harmony. *Nat. Methods* **16**, 1289–1296 (2019).
131. Traag, V. A., Waltman, L. & van Eck, N. J. From Louvain to Leiden: guaranteeing well-connected communities. *Sci. Rep.* **9**, 5233 (2019).
132. Alquicira-Hernandez, J. & Powell, J. E. Nebulosa recovers single-cell gene expression signals by kernel density estimation. *Bioinforma. Oxf. Engl.* **37**, 2485–2487 (2021).
133. Cummins, C. L. et al. Liver X receptors regulate adrenal cholesterol balance. *J. Clin. Invest.* **116**, 1902–1912 (2006).
134. Schindelin, J. et al. Fiji: an open-source platform for biological-image analysis. *Nat. Methods* **9**, 676–682 (2012).
135. Rueden, C. T. et al. ImageJ2: imageJ for the next generation of scientific image data. *BMC Bioinformatics* **18**, 529 (2017).
136. Bray, N. L., Pimentel, H., Melsted, P. & Pachter, L. Near-optimal probabilistic RNA-seq quantification. *Nat. Biotechnol.* **34**, 525–527 (2016).
137. Soneson, C., Love, M. I. & Robinson, M. D. Differential analyses for RNA-seq: transcript-level estimates improve gene-level inferences. *F1000Research* **4**, 1521 (2015).
138. Robinson, M. D., McCarthy, D. J. & Smyth, G. K. edgeR: a Bioconductor package for differential expression analysis of digital gene expression data. *Bioinformatics* **26**, 139–140 (2010).
139. Leek, J. T., Johnson, W. E., Parker, H. S., Jaffe, A. E. & Storey, J. D. The sva package for removing batch effects and other unwanted variation in high-throughput experiments. *Bioinforma. Oxf. Engl.* **28**, 882–883 (2012).
140. Ritchie, M. E. et al. limma powers differential expression analyses for RNA-sequencing and microarray studies. *Nucleic Acids Res.* **43**, e47 (2015).

Acknowledgements

Research reported in this publication was supported by the International Fund for Congenital Adrenal Hyperplasia to G.D.H., F.B., and T.D., the Center for Cell Plasticity and Organ Design to T.D., the National Institutes of Health/National Institute of Diabetes and Digestive and Kidney Diseases of the National Institutes of Health under Award Number R01DK043140, R01DK062027 to G.D.H. and Dr. William Rainey, the National Heart, Lung, and Blood Institute under Award Number 1R01HL15583401 to A.F.T., the Swiss National Science Foundation (310030L_182700/1) to F.B., the Swiss NCCR "Kidney.CH" and from the University Research Priority Program of the University of Zurich ITINERARE–Innovative Therapies in Rare Disease to D.P. and F.B. The content is solely the responsibility of the authors and does not necessarily represent the official views of the National Institutes of Health. We thank all the members of the Hammer Lab for helpful discussion and feedback on the manuscript. We especially thank Dr. Rainey (University of Michigan) for providing Human adrenal paraffin samples and sharing ARKO RNAseq. We thank Dr. Pierre Val (University of Clermont-Ferrand) for sharing reagents. We thank Dr. Gregg Myers (University of Michigan) for technical assistance with hematopoietic cells. We thank Dr. Leonard Cheung (Stony Brook University) for helpful discussion regarding HHEX expression in the mouse pituitary gland. We thank Dr. Klionsky (University of Michigan), autophagy expert for helpful discussion on lipophagy process. We thank Dr. Frank Claessens and Dr. Johan Swinnen (KU Leuven) for sharing the *AR* flox mice[60]. The research reported in this publication used the Advanced Genomic Core, the Microscopy Core, the Flow Cytometry Core, and the Orthopaedic Research Laboratories (ORL) Histology Core at the University of Michigan. We especially thank Emma Snyder-White and Carol Whitinger for technical assistance with histology experiments and Michael Pihalja with FACS sorting.

Author contributions

We followed guidelines for authorship at University of Michigan Office of Research including 4 criteria. (1) significant contribution to the conception or design of the work; or the acquisition, analysis, or interpretation of data for the work; (2) drafting the work or revising it critically for important intellectual content; (3) final approval of the version to be published; (4) agreement to be accountable for all aspects of the work in ensuring that questions related to accuracy or integrity of any part of the work are appropriately investigated. T.D., K.J.B., and G.D.H. design the experiments, T.D. and A.M.L. analyzed the data, T.D., K.J.B., M.C.F., C.R.L., D.J, E.S., and K.A.H. genotyped mice, performed the experiments, or acquired data. C.L. and A.F.T. performed LCMSMS. S.W.P. and A.M.L. analyzed the ARKO RNAseq data. D.P. and F.B. provided *Cyp11b1-Cre*^{ERT2} mice. D.T.B. provided *Cyp11b2-Cre* (AS-Cre) mice. T.D. wrote the original manuscript, T.D., K.J.B., C.R.L., and G.D.H. edited the manuscript. All coauthors provided expertise and feedback.

Competing interests

G.D.H. Founder and Board of Directors—Sling Therapeutics, Advisor—Orphagen Pharmaceuticals. The remaining authors declare no competing interests.

Additional information

Supplementary information The online version contains supplementary material available at https://doi.org/10.1038/s41467-025-68257-4.

Correspondence and requests for materials should be addressed to Typhanie Dumontet.

Peer review information *Nature Communications* thanks the anonymous reviewers for their contribution to the peer review of this work. A peer review file is available.